

CONTINUOUS-FLOW PHOTOCATALYTIC REACTOR FOR THE
PRECISELY CONTROLLED DEPOSITION OF METALLIC
NANOPARTICLES

By
MIRSAJJAD MOUSAVI

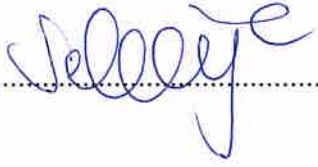
Submitted to the Graduate School of Engineering and Natural Sciences
in partial fulfillment of
the requirements for the degree of
Master of Science

Sabanci University
Summer 2019

A CONTINUOUS-FLOW PHOTOCATALYTIC REACTOR FOR THE
PRECISELY CONTROLLED DEPOSITION OF METALLIC
NANOPARTICLES

APPROVED BY:

Prof. Dr. Selmiye Alkan Gürsel
(Thesis Supervisor)



.....

Assoc. Prof. Dr. Önder Metin



.....

Asst. Prof. Dr. Alp Yürüm



.....

DATE OF APPROVAL: 18/07/2019

© Mirsajjad Mousavi 2019
All Rights Reserved

ABSTRACT

A CONTINUOUS-FLOW PHOTOCATALYTIC REACTOR FOR THE PRECISELY CONTROLLED DEPOSITION OF METALLIC NANOPARTICLES

Mirsajjad Mousavi

Materials Science and Nano-Engineering, M.Sc. Thesis 2019

Supervisor: Prof. Dr. Selmiye Alkan Gürsel

Keywords: Platinum nanoparticles, Gold nanoparticles, TiO₂ nanocomposite, Metallic nanoparticles, Partially reduced graphene oxide, Photocatalytic deposition, Continuous-flow reactor, Photodeposition

Abstract: In this project, applicability of photodeposition of different noble metal nanoparticles on various photocatalyst materials by means of a novel continuous-flow photocatalytic reactor has been studied. Three different composite systems (Pt/graphene, Pt/TiO₂, and Au/TiO₂) with monodisperse and uniformly distributed particles were produced by this reactor, and the photodeposition mechanism, as well as the synthesis optimization strategy, were discussed. By the pulsed and controlled excitation of the photocatalyst, precise deposition of metallic nanoparticles on photocatalyst substrate was achieved. Guidelines for the replication of the reactor and its operation were provided in detail. The synthesis methods and their technical aspects were described comprehensively. The role of the ultraviolet (UV) dose on the photodeposition process and exposure length were investigated and the characteristic photodeposition behavior of each composite system were provided. To characterize the final products, FE-SEM, TEM, XPS, and ICP-OES were used to identify morphology, size distribution, composition, and photodeposition reaction ratio, respectively. Although our current work does not yield a comprehensive strategy with optimized parameters

of photodeposition for the abovementioned nano-composite systems, capability of the developed continuous-flow photocatalytic reactor for TiO₂ semiconductor substrate with platinum and gold noble metals was proved, and knowledge was enriched.

ÖZET

METALİK NANOPARÇACIKLARIN TAM KONTROLLÜ BIRIKTIRMESİ İÇİN KULLANILAN SUREKLI AKIŞLI FOTOKATALİK BİR REACTÖR

Mirsajjad Mousavi

Malzeme Bilimi ve Nano-Mühendisliği, Yüksek Lisans Tezi 2019

Danışman: Prof. Dr. Selmiye Alkan Gürsel

Keywords: Platin nanoparçacıklar, Altın nanoparçacıklar, TiO₂ nanokompozit, Metalik nanoparçacıklar, Kısmen indirgenmiş grafen oksit, Fotokatalitik biriktirme, Sürekli akışlı reaktör, Fotobiriktirme

Abstract: Bu projede, yeni sürekli akışlı fotokatalitik reaktör yardımı ile birçok fotokatalitik malzeme üzerine farklı soy metal nanoparçacıklarının fotobiriktirme uygulanması çalışıldı. Tekil ve homojen bir şekilde dağılmış parçacıklar içeren üç farklı kompozit sistem (Pt/ grafen, Pt/ TiO₂ ve Au/ TiO₂) bu reaktör tarafından üretildi ve sentez optimizasyonu stratejisinin yanısıra fotobiriktirme mekanizması da tartışıldı. Fotokatalistin atma ve kontrollü uyarılması ile fotokatalist altlık üzerine metalik nanoparçacıkların tam biriktirilmesi gerçekleştirildi. Reaktörün tekrarlı üretimi ve çalışması için genel bilgiler ayrıntılı olarak verildi. Sentez metodu ve teknik bilgiler değişik açılardan kapsamlı olarak açıklandı. Ultraviyole (UV) dozunun fotobiriktirme işlemi ve maruz kalma uzunluğu üzerindeki rolü araştırıldı ve her bir kompozit sistemin karakteristik fotobiriktirme davranışı sağlandı. Son ürünü karakterize etmek amacıyla; morfoloji, parçacık boyutu dağılımı, kompozisyon ve fotobiriktirme reaksiyonu oranını belirlemek için sırasıyla FE-SEM, TEM, XPS, ve ICP-OES kullanıldı. Şu andaki çalışmamız, yukarıda belirtilen nano-kompozit sistemler için optimize edilmiş fotobiriktirme

parametreleri ile kapsamlı bir strateji sunmamasına rağmen, platin ve altın gibi soy metallerle TiO₂ yarı iletken altlık için geliştirilen sürekli akışlı fotokatalitik reaktörün kabiliyeti kanıtlandı ve bilgi zenginleştirildi.

Acknowledgment

I would like to express my sincere appreciation and gratitude to my supervisor, Professor Dr. Selmiye Alkan Gürsel for her productive knowledge and supportive guidance throughout the thesis. Her strong support from any personal and professional prospective motivated me during this project.

My sincere gratitude to my thesis defense jury members who have reviewed this dissertation with meticulous consideration.

Finally, yet importantly, I would like to appreciate the great support of my dear wife and my lovely parents who I owe them my life and all my achievements.

Dedication

I would like to dedicate this thesis to my beloved wife Sanaz Abbasi for her endless support, to my parents Mr. Mirmasoud Mousavi, and Mrs. Roghayeh Jamshidi for keeping me spirit up, and to my brother Mr. Mirsobhan Mousavi.

Table of Content

1	Introduction	3
1.1	Photodeposition: Definition and History.....	3
1.2	Principles and Applications of Photodeposition of Metal (Oxide) Nanoparticles on Semiconductor Surface.....	4
1.3	Nanoparticles Photodeposition on TiO ₂	6
1.3.1	Effect of pH	6
1.3.2	Effect of Metallic Precursor.....	8
1.3.3	Effect of Existence of Oxygen and Hole Scavengers.....	9
1.4	Nanoparticles Photodeposition on ZnO	10
1.5	Photodeposition of Nanoparticles on Graphene	14
1.6	Nanoparticles Photodeposition on Other Metal Oxides.....	17
1.6.1	Gallium Oxide.....	17
1.6.2	Bismuth Vanadate, BiVO ₄	19
1.6.3	Tantalum Oxide, Ta ₂ O ₅	21
1.6.4	Strontium Titanate, SrTiO ₃	22
2	Objective of This Work	25
3	Materials and Methods.....	27
3.1	Design of Photocatalytic Deposition Reactor.....	27
3.2	Supplying the Reactants to the Continuous-flow Photodeposition Reactor.....	28
3.3	Synthesis Procedures.....	29
3.3.1	Synthesis of GO	29
3.3.2	Synthesis of Partially Reduced GO (PRGO)	29
3.3.3	Photocatalytic Deposition of Platinum on PRGO	30
3.3.4	Photocatalytic Deposition of Platinum/Gold on TiO ₂	30
3.4	Samples Characterization Methods.....	30
4	Results and discussion	33
4.1	Morphological Investigation by Field-Emission Scanning Electron Microscopy...33	
4.2	X-ray diffraction for Reduction Confirmation	36
4.3	Surface area and pore size analyses of Anatase TiO ₂	37
4.4	Transmission Electron Microscopy for Size Distribution and Morphology	38
4.5	X-ray Photoelectron Spectroscopy for the Reduction Confirmation.....	40
4.6	Inductively Coupled Plasma-Optical Emission Spectrometry (ICP-OES) for Monitoring Photodeposition Rate.....	42
5	Conclusions.....	46
6	References	48

List of Figures

Figure 1. An overview of increasing number of published papers in scientific journals between 1982-2019. The data was extracted from Scopus on July, 07, 2019.....	3
Figure 2. Schematic of (a) reductive photodeposition and (b) oxidative photodeposition; VB: valence band, CB: conduction band, D: e- donor, A: e- acceptor [2].....	4
Figure 3. Schematized review of reaction occurred for in-situ photodeposition: Reduction of a metal cation (k1) on the photocatalyst surface, parallel to the reduction of H ⁺ ions to produce H ₂ (k2). When the concentration of the metal cation decreases to zero level, the amount of loading for a specific metal can be calculated from hydrogen evolution. D is the sacrificial reagent utilized as the hole scavenger [18].....	5
Figure 4. First obtained photodeposition rates for different Pt precursor solutions on the surface of TiO ₂ in various conditions [43].....	9
Figure 5. Schematically illustration of (a) functionalized graphene, NEG-decorated; (b) when all NEGs are off, dark mode; (c) NEG-decorated (functionalized) graphene under UV illumination, starting point of Pt nanoparticles growth. The yellow and blue colored atoms have hybridizations of sp ³ and sp ² , respectively.	16
Figure 6. in-situ measurement of H ₂ production while the photodeposition of Rh on Zn-loaded Ga ₂ O ₃ [14].....	18
Figure 7. Characteristic XPS spectrum of the Cr 2p and the Cu _{LMM} Auger region of the samples of 0.4 wt% Cu on Ga ₂ O ₃ and 0.09 wt% Cr 0.4 wt% Cu on Ga ₂ O ₃ [72].....	19
Figure 8. Auger electron spectrum of different concentration of Ag/BiVO ₄ by impregnation and photodeposition. a) 1.3 wt.% Ag/BiVO ₄ by impregnation. b) 1.3 wt.% Ag/BiVO ₄ by impregnation in the exposure of H ₂ stream for 1 hr at 353 K. c) 2 wt.% Ag/BiVO ₄ by photodeposition [78].....	20
Figure 9. Photodecomposition behavior of RhB in aqueous media with and without Au nanoparticles, a) without photocatalyst, b) 1.0 wt% of Au-Ta ₂ O ₅ c) 1.0 wt% of Au-Ta ₂ O ₅ under visible light illumination [79].....	21
Figure 10. X-ray photoelectron spectrum of Ag nanoparticles photodeposited on SrTiO ₃ nanotube substrate. a) wide scan spectrum b) Deconvoluted spectra for Ag 3d [90].....	23
Figure 11. Schematically detailed illustration of the photocatalytic deposition reactor. The N ₂ gas outlet form the suspension conducted to the bubbler through T ₁ pipe. The Ps point is the sample collection point in different times (the ending point of T ₂ tube). V ₀ , V ₁ , and V ₂ are the valves for initial feeding, sampling and tube evacuation, respectively [91].....	28
Figure 12. FE-SEM images of photodeposited catalytic nano-composites with 20% exposure length with different concentration ratio of noble metal over substrate, a) 7% wt. Au/TiO ₂ with 4 UV lamps b) 7% wt. Au/TiO ₂ with 2 UV lamps c) 5% wt. Au/TiO ₂ with 4 UV lamps d) 5% wt. Au/TiO ₂ with 2 UV lamps e) 7% wt. Pt/TiO ₂ with 4 UV lamps f) 7% wt. Pt/TiO ₂ with 2 UV lamps g) 5% wt. Pt/TiO ₂ with 4 UV lamps h) 5% wt. Pt/TiO ₂ with 2 UV lamps i) 2% wt. Au/TiO ₂ with 2 UV lamps j) 2% wt. Pt/TiO ₂ with 2 UV lamps k) untreated TiO ₂	35
Figure 13. X-ray diffraction patterns of graphite, graphene oxide, and partially reduced graphene oxide.	36
Figure 14. X-ray diffraction patterns of Pt-reduced graphene oxide 120-60%, Pt-reduced graphene oxide 120-20%, and Au-reduced graphene oxide.	37
Figure 15. Nova e-series surface area and pore size analyzer from Quantachrome Instruments.	37
Figure 16. Pore size distributions of Anatase TiO ₂ by using BJH method.....	38

Figure 17. TEM images. (A) Pt/graphene composite produced by a 100% exposure tube (this figure has been modified from Abdolhosseinzadeh *et al.* [70]. (B) Au/TiO₂. (C) Pt/TiO₂. (D) Effect of a high IDE in the formation of large particles and the depletion of its surroundings in Pt/graphene composite.....39

Figure 18. XPS survey spectra. Spectra for the (A) Pt/TiO₂ composite, and (B) Au/TiO₂ composite. Deconvoluted spectra for (C) Pt4f in the Pt/TiO₂ composite, and (D) Au4f in the Au/TiO₂ composite.....41

Figure 19. Concentration changes of the metallic cations during the PD in the developed reactor with various IDEs. Changes in (A) Pt/graphene, (B) Au/TiO₂, and (C) Pt/TiO₂.....42

List of Tables

Table 1. Effect of UV exposure length on photodeposition rate of Pt on graphene and effect of UV illumination power on photodeposition rate of Au/Pt on TiO ₂	43
---	----

Introduction

1 Introduction

1.1 Photodeposition: Definition and History

Deposition of metal/ metal oxide nanoparticles on the surface of a semiconductor is achieved by illumination of the desired metal salt aqueous solution containing an amount of the semiconductor slurry. This process is called photodeposition, and it was conducted for the first time by Clark and Vondjidis in 1965 [1]. They showed that using infrared light causes the illumination of silver nitrate and titanium oxide mixture, which results in the formation of the metallic silver. However, a later research carried out by Kraeutler and Bard [2] in 1978 was known as the best promising study in the field of photodeposition. In their work, illumination was performed on a slurry of hexachloroplatinic acid (H_2PtCl_6), hydrochloric acid (HCl), acetic acid (as an electron donor), sodium carbonate and anatase powder to load platinum (Pt) on the titanium dioxide (anatase TiO_2) surface (Figure 2a). Reaction was carried out at 55 °C under nitrogen atmosphere to remove any remaining O_2 and CO_2 . Obtained results confirmed a very good dispersion of Pt nanoparticles. Since that time, because of applicability, efficiency, and cost-effectivity of research aims, researchers got interested in focusing on photodeposition and photocatalyst materials. In figure 1. An overview of increasing number of published papers in scientific journals since 1982 was presented. It does worth to mention that; all related published articles are not included since photodeposition is not the only one name in this field of research.

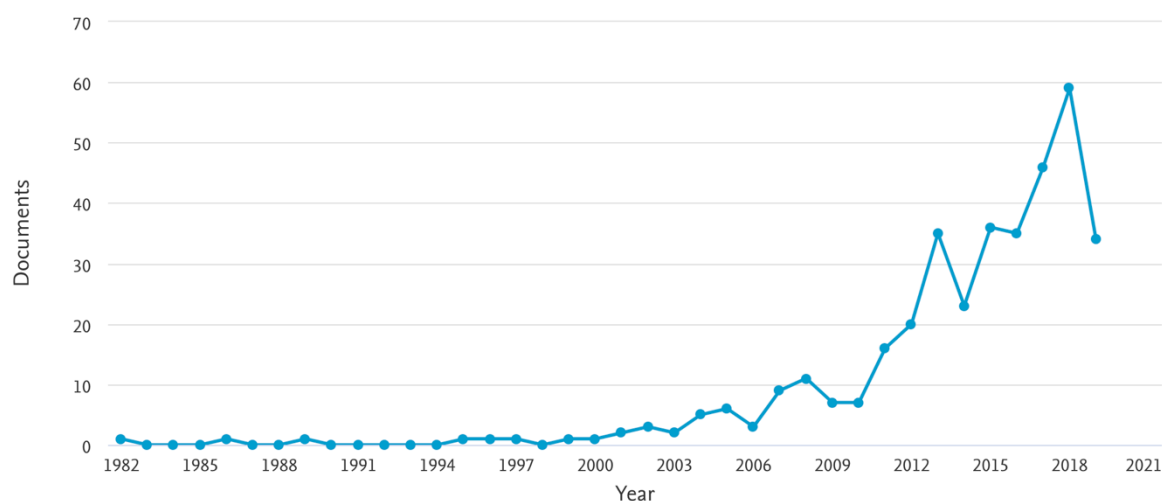


Figure 1. An overview of increasing number of published papers in scientific journals between 1982-2019. The data was extracted from Scopus on July, 07, 2019.

1.2 Principles and Applications of Photodeposition of Metal (Oxide) Nanoparticles on Semiconductor Surface

The principle of photodeposition is based on the electrochemical reaction induced by light. The general reaction for a metal reductive photodeposition is presented in Eq.1 where M is the metal component and n is the number of electrons.



Eq.2 represents the oxidation reaction for metal oxide nanoparticles photodeposition.



Figure 2. provides an overview of both reductive and oxidative photodeposition phenomena.

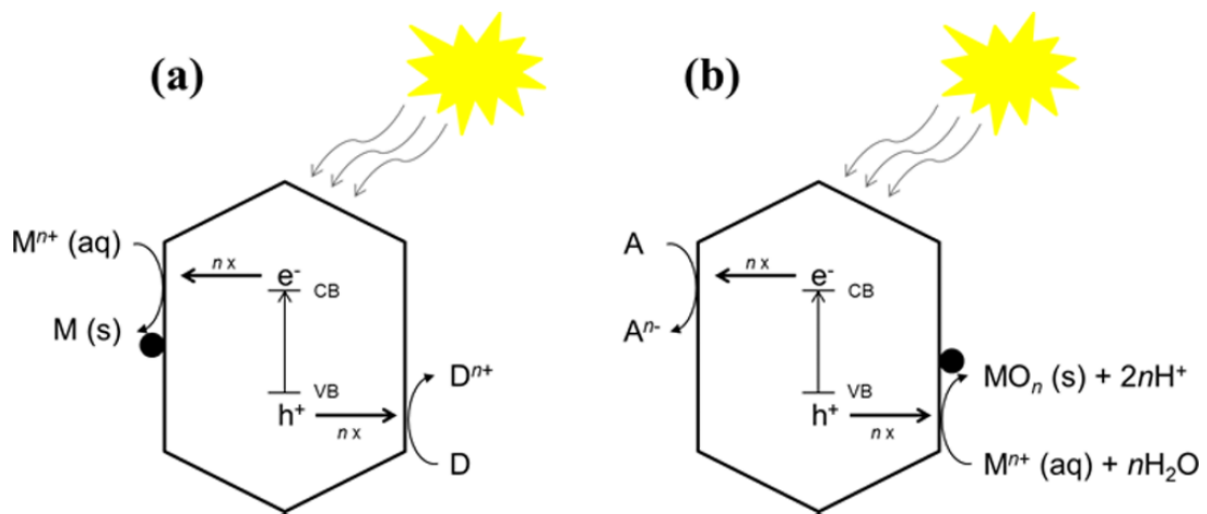


Figure 2. Schematic of (a) reductive photodeposition and (b) oxidative photodeposition; VB: valence band, CB: conduction band, D: e- donor, A: e- acceptor [2].

For a successful photodeposition, the reduction/oxidation potential of the metal oxide and the energy level of the semiconductor's available position must be in a favorable range. This means that the energy level of CB (in the scale of E vs. NHE (normal hydrogen electrode) should be more negative than the metals' reductive potential. Also, the energy of VB must be more positive (E vs. NHE scale) than the oxidation potential of metal ions, sacrificial agents or water. During the process of photodeposition, it is necessary that the intensity of incident light exceeds the energy of the semiconductor band-gap. Efficient separation and migration of charge carriers is the next important step. Finally, the semiconductor must provide enough active surface to make the photodeposition possible. Since the composition of metal precursors in aqueous and dry state could be changed, differences in preparation time, reactivities, and the morphology

of obtained nanoparticles are expectable. Metal oxide nanoparticles photodeposited on semiconductor surfaces are widely used for application such as synthesis of photocatalytic solar fuel [3-5], air purification and wastewater treatment [6, 7].

In addition to photodeposition, there are other methods that are applied for cocatalytic nanoparticles deposition on the high surface areas of semiconductor. These methods include physical mixing [8], chemical reduction [9, 10], impregnation [11], electrodeposition [10], sputtering [12] and atomic-layer deposition (ALD) [13]. However, the aforementioned techniques are either effective at high operating temperature ranges or at an applied (bias)potential. This makes photodeposition as the most attractive method, due to the facilitate creation of cocatalyst nanoparticles in the slurry reactor by illumination as the only required condition.

Favorable properties of photodeposition are controlled distribution of nanoparticles on the crystals of facet-engineered semiconductors with respect to geometry, and consequently controlling the oxidation state and size of the deposited nanoparticles.

Optimization of cocatalyst nanoparticles loading is very important in photocatalysis procedure for water splitting [14-17]. For this purpose, in-situ observation of H₂ formation in the photodeposition is applied. The reactions occurred during the in-situ deposition is shown in Figure 3 [18].

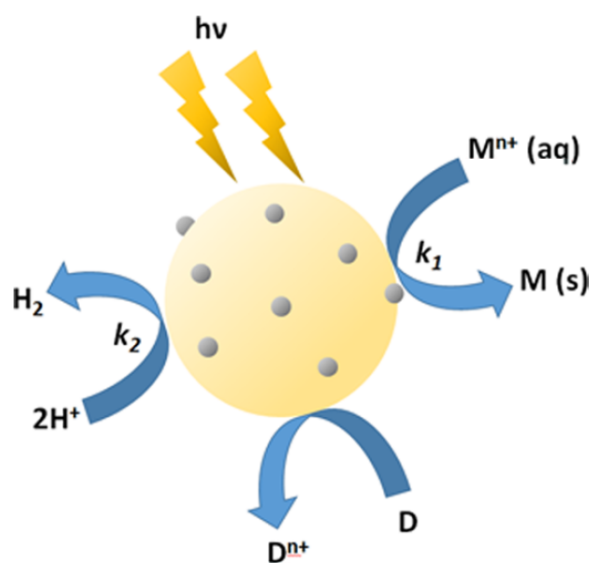


Figure 3. Schematized review of reaction occurred for in-situ photodeposition: Reduction of a metal cation (k_1) on the photocatalyst surface, parallel to the reduction of H^+ ions to produce H_2

(k2). When the concentration of the metal cation decreases to zero level, the amount of loading for a specific metal can be calculated from hydrogen evolution. D is the sacrificial reagent utilized as the hole scavenger [18].

Semiconductors with deposited cocatalysts prepared through photodeposition or other deposition methods show different performance behaviors. This can be due to the variations in the deposited metal oxide nanoparticle sizes, oxidation states and the amounts of agglomeration achieved by applying each different technique. These characteristics are the main determining factors for the performances attained from different preparation methods.

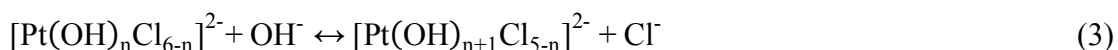
1.3 Nanoparticles Photodeposition on TiO₂

Many researches have been dedicated to nanoparticles photodeposition on TiO₂ surface. Investigated nanoparticles mostly include noble metals, for example platinum (Pt) [19-24], silver (Ag) [25], gold (Au) [26, 27], and palladium (Pd) [28, 29], also a number of metal oxides ; PbO₂ [30], RuO₂ [31] or composite nanoparticles such as CoPi, a catalyst containing cobalt and in-organic phosphate used for water oxidation reaction [32].

Furthermore, some works were dedicated to the photodeposition study of CdS, a different semiconductor, on TiO₂. The application of photodeposition in the preparation of different materials such as particles with core-shell structure [33-36], bimetallic [37, 38], and trimetallic cocatalyst using additional annealing [38] has also been developed. Several works focused on the optimization of cocatalyst weight loading to achieve higher photocatalytic activity in photodeposition. In the following, the effects of pH, metallic precursors and existence of oxygen and hole scavengers were investigated to optimize photodeposition of novel metallic elements on TiO₂ [38-41].

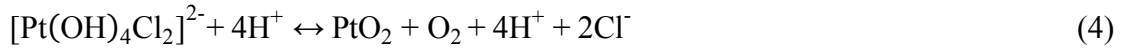
1.3.1 Effect of pH

Composition and morphology of the deposited Pt particles are significantly dependent on pH. Xi *et al.* [42] stated that in an oxygen-free photodeposition, [PtCl₆]²⁻ (n=0 for Eq. 3) is hydrolyzed as the following:



Where n can take the values of 0-5. According to this equilibrium reaction, it is implied that at high pH values, a considerable fraction of OH ligands are present in the Pt precursor. This can affect the kinetics of both of oxidation state and photodeposition of achieved Pt nanoparticles. This occurrence was also confirmed in the presence of anatase photodeposited Pt(OH)₂ at

neutral and low pH, and the existence of additional PtO₂ in high pH. The hypothesis was that PtO₂ is possibly formed in the following reaction (Eq.4), assisted by the oxidation of hydroxyl groups present in the already adsorbed complex [Pt(OH)₄Cl₂]²⁻:



The reduction reaction of [Pt(OH)₄Cl₂]²⁻ in Eq.5 was suggested for Pt(OH)₂ formation:



Using XPS, it was proved that at constant photodeposition time, compared to the results obtained from high pH values, lower amounts of Pt were deposited when performing the reaction at low pHs. Moreover, adding an excessive amount of Cl⁻ (in NaCl form) at low pH resulted in no Pt deposition at all, thus considered to have a destructive effect on the photodeposition.

The destructive effect of adding Cl⁻ during the Pt deposition in low pH on the surface of Evonik-Degussa P25 was also observed by Mahlamvana and Kriek [43] for [PtCl_n(H₂O)_{4-n}]²⁻ⁿ (n = 0-4). They discovered that without using any sacrificial agent, no Pt photodeposition occurred when only [PtCl₄]²⁻ was in the solution.

Expectedly, this chemical condition is totally changed when there is indeed a sacrificial agent present in the solution. Despite the previous works of Xi *et al.* [42] and Mahlamvana and Kriek [43], the research conducted by Zhang *et al.* showed a significantly high Pt photodeposition rate at low pH on the nanoporous surface of Degussa P25 by using ethanol. The obtained rate of photodeposition was even higher than that achieved at high pH value.

Zhang *et al.* [44] brought up the electrostatic interactions as an explanation for the deposition rate difference at low and high pH values while using a sacrificial agent. According to his work, when the pH value is lower than TiO₂'s isoelectric point (IEP = 6.25), there is an attraction between the Pt complex negative charges in the solution and the positive charges on the surface of TiO₂. This results in a desired amount of adsorption (high deposition rate) with a wide range of nanoparticles size. It was apparent that electrostatic interactions were the major role players

only when a sacrificial agent is used in the solution. Accidentally, a huge amount of Pt nanoparticle agglomerations was obtained at pH values close to the IEP of TiO₂.

In conclusion and also by taking into account the work done by Xi *et al.* [42] the effect of pH on the oxidation state is significant regardless of the sacrificial agent presence. Results showed the formation of metallic Pt and PtO₂ at pH < 5 and >9, respectively. The presence of Pt and PtO at pH = 5-7 and PtO and PtO₂ at pH =7-9 were observed. Both Xi *et al.* [42] and Zhang *et al.* [44] contributed this results [PtCl₆]²⁻ hydrolysis reaction (Eq.3)

Apparently, electrostatic interactions are particularly relevant when a sacrificial agent is present in solution. Incidentally, around the pH value of the isoelectric point of TiO₂, large agglomerates of Pt particles were found. Generally, in agreement with Xi *et al.* even in the presence of a sacrificial agent the oxidation state is dependent on pH: metallic Pt⁰ was formed at a pH lower than 5, and PtO₂ was formed at pH values higher than 9. In the pH range 5– 7, both Pt and PtO were found, and in the pH range 7– 9, both PtO and PtO₂ were found. Just as in Xi *et al.*, Zhang *et al.* [44] attributed this phenomenon to hydrolysis of the [PtCl₆]²⁻ precursor (eq. 3).

1.3.2 Effect of Metallic Precursor

Pt precursor effect on the metal photodeposition rate on TiO₂ (nanoporous surface of Degussa P25) was studied by Herrmann *et al.* [45] in anerobic environment and without using any sacrificial agent. Compounds [PtCl₆]²⁻(H₂PtCl₆), Na₂PtCl₆, H₂Pt(OH)₆ and Pt(NO₂)₂(NH₃)₂ were used as Pt precursors. Among all precursor materials, photodeposition rate obtained from using Pt(NO₂)₂(NH₃)₂ was considerably lower. This was attributed to the nonionic nature of the compound, which results in a small adsorption coefficient value. Remarkably, the deposition rates obtained from H₂Pt(OH)₆ and solutions containing chlorine are somewhat similar. According to the research conducted by Xi *et al.* [42] although the pH values of the solutions are not clear, it is predicted that for precursor solutions containing [PtCl₆]²⁻ with existence of chloride, lower pH values cause low deposition rates.

Au photodeposition with methanol presence on the surface of Degussa P25 was also addressed [26]. Like Pt, the average size of the deposited Au particles is comparatively small at high pH conditions; 18 nm and 4 nm at pH values of 3 and 9, respectively. Consequently, best photocatalytic activity for degradation of oxalic acid was achieved by preparation of

photodeposited Au nanoparticles at $\text{pH} > 7$. But unlike Pt, Au particles went through reduction by photodeposition process, regardless of the solution pH.

In a different research, the variation between the photodeposition process of Pt and Pd was also investigated. In the work carried out by Mahlamvana and Kriek [40], it was shown that Cl^- has a detrimental effect on the $[\text{PtCl}_n(\text{H}_2\text{O})_{4-n}]^{2-n}$ ($n = 0-4$) photodeposition rate on the surface of Evonik-Degussa P25. For the same semiconductor material, the photodeposition was performed much faster by using $\text{PdCl}_2(\text{H}_2\text{O})_2$. This suggest an optimum balance between Cl^- and water ratio which can influence the electrostatic interactions.

1.3.3 Effect of Existence of Oxygen and Hole Scavengers

It was demonstrated by Mahlamvana and Kriek [43] that oxygen presence has a detrimental influence on Pt deposition rate on Evonik-Degussa P25 (a TiO_2 compound). They claimed that oxygen competes as a scavenger for electron. Also, it was demonstrated that using an oxygen-free gas to purge the photoreactor greatly depended on the precursor type. The order of least to most effective precursor without using oxygen gas was $[\text{PtCl}_4]^{2-} < [\text{PtCl}_3(\text{H}_2\text{O})]^- < \text{H}_2\text{PtCl}_6 < \text{K}_2\text{PtCl}_6$ ($[\text{PtCl}_4]^{2-}$ had no photodeposition reactivity.) (Figure 4).

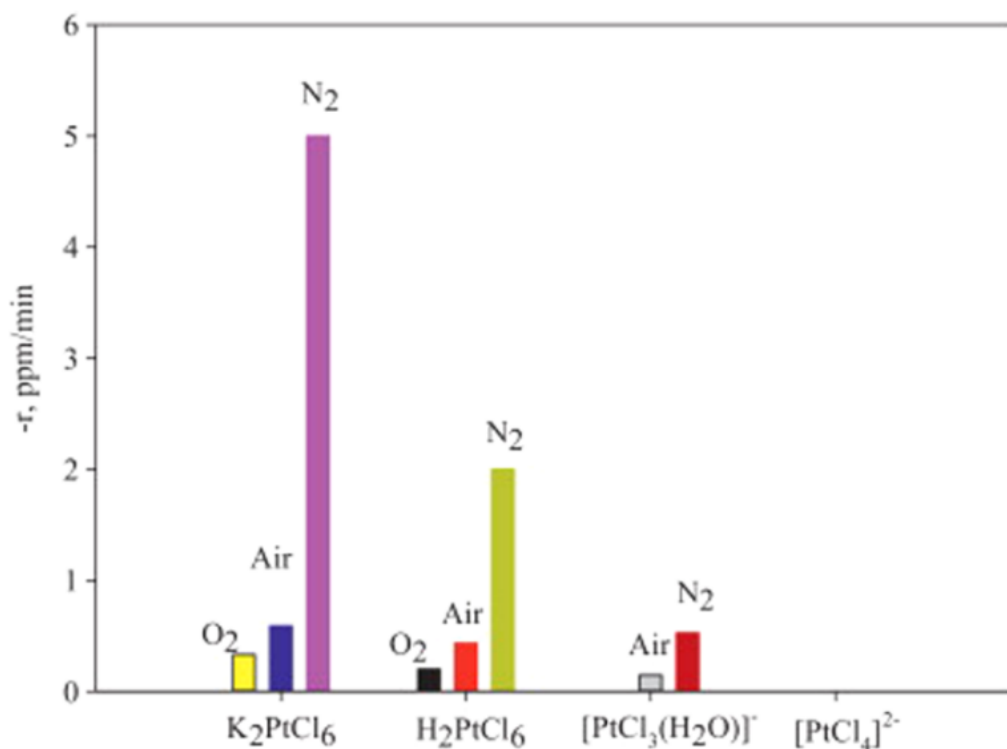


Figure 4. First obtained photodeposition rates for different Pt precursor solutions on the surface of TiO_2 in various conditions [43].

Regarding Degussa P25, Borgarello *et al.* [29] also stated the same negative effect of oxygen on RhIII's reduction degree. Most possibly this effect is caused by the competition between oxygen and RhIII for reduction reaction. By taking into account the previous results as well, it can be concluded that for completing the reduction of Rh, Pt and Pd, methanol should be used as a sacrificial agent. Additionally, a number of studies were dedicated to the relation between the sacrificial agent type and photodeposition rate. This was proved for the case of Rh deposition on TiO₂ (calcinated anatase). The effect of sacrificial agent type is ordered from low to high as the following: 2-propanol < 1-propanol << ethanol < methanol [46]. Repeatedly, this can be considered as the relation outcome between the mentioned alcohol derivatives and the radicals' reduction potential which were formed from the hole-transfer reactions.

1.4 Nanoparticles Photodeposition on ZnO

The presence or absence of a sacrificial agent has as much as a strong effect on the morphology and photodeposition rate of Ag on ZnO as it does for TiO₂. Using a glass substrate, Liu *et al.* [47] investigated the influence of ethanol as a sacrificial agent in Ag photodeposition on the nanorods of ZnO in aqueous solution.

The existence of ethanol in the precursor considerably enhanced the rate of photodeposition, and as its result a large number of Ag nanoclusters (500-600 nm long) were deposited on the outer surface of ZnO nanorods. The changes caused by ethanol can be contributed to the change in adsorption behavior of ZnO with regards to Ag⁺, which may affect Zn-O-C₂H₅ species formation on the surface. By using ethanol in the photodeposition procedure under visible light condition, the obtained photocatalytic activity intended for the degradation of Rhodamine B (RhB) was much lower than required. This could be attributed to 1) blocking the available reaction sites for RhB by Ag, 2) Ag preventing the Ag/ZnO interface from getting access to visible-light, thus decreasing the state amounts of surface plasmon resonance and consequently reducing the photocatalytic activity.

Similarly, Huang *et al.* [48] brought up the attention to the influence of sacrificial agents on the rate of photodeposition and morphology of Ag nanoparticles on ZnO. They carried out Ag photodeposition on the surface of ZnO nanoflowers by using three different solutions of AgNO₃: 1) without any sacrificial agent, 2) with ethanol as the sacrificial agent and 3) containing glycol as the sacrificial agent. The achieved deposited Ag contents were 27.6, 23.6

and 35.0 weight percent, respectively. It is worth mentioning that despite an increased rate of photodeposition by using glycol, the same outcome was not observed for ethanol. However, ethanol indeed increased the size of deposited Ag nanoparticles (100 nm and 10 nm for the presence and absence of ethanol, respectively). It was stated that the preparation of Ag/ZnO composites by using glycol in the photodeposition presented best dye photocatalytic degradation.

In the work of Wang *et al.* [49] Ag photodeposition on the surface of ZnO tetrapod whiskers was explored at different poly(ethylene glycol) (PEG) concentrations in the aqueous solution of AgNO₃. With keeping the illumination intensity constant and increasing PEG concentration, an increase in the rate of Ag nanoparticles deposition and a decrease in the average size of the nanoparticles were observed. Additional interesting fact in their study was the acclaimed independency of Ag⁺ reduction reaction to the formed electrons in ZnO. In fact, it was stated that formed OH• radicals through ZnO are captured by PEG which produces acid or aldehyde. Afterwards, acid or aldehyde compounds assist the reduction of Ag⁺ to Ag.

The dependency of Ag nanoparticles morphology to the illumination time was studied by some researchers. It was observed by Lin *et al.* that by increasing the time of illumination, both the quantity and size of Ag nanoparticles were larger. Although the increase in particle size was moderate; 13.4 nm for 5 min and 15.9 nm for 25 min of irradiation. Similar but increased behavior was achieved through the work of Li *et al.* They obtained 11 nm nanoparticles for 30 min and 29 nm for 8 h of irradiation. It was also shown that the increased quantity of photodeposited Ag nanoparticles resulted in improved performance for sensing SERS and H₂O₂-based Rhodamine 6G.

Peng *et al.* and Behnajady *et al.* [50] studied the photodegradation of methyl orange by Ag/ZnO composites. They noticed that for longer irradiation times, there is an initial increase in Ag/ZnO performance. However, when the deposition time is extended beyond a certain point, the performance behavior becomes constant for the deposited nanoparticles. They have logically contributed this phenomenon as a result of Ag⁺ complete reduction to Ag.

It is noteworthy to mention that photocatalytic activity enhancement of ZnO with deposited Au or Pd nanoparticles is related to the increased separation of charge-carrier and improved electron-transfer rates.

Photodeposition rates and morphology behavior of Pd or Au on the surface of ZnO is similar to that of Pt on TiO₂. Both properties depend on 1) existence or nonexistence of a sacrificial agent, 2) pH value, 3) conditions of illumination and 4) illumination time. The typical precursor used for Au nanoparticle's preparation is [AuCl₄]⁻, though in some cases it was also performed using potassium gold cyanide. Ethanol and methanol were utilized as sacrificial agents. Methanol showed enhanced rate of photodeposition for Au in the research conducted by Park *et al* [51].

The structure of 1 wt.% Au particles and their catalytic activity for CO oxidation was investigated by Carabinero *et al.* [52] They studied the effect of irradiation time, pH and ZnO morphology on the photodeposition and compared the results to those obtained from other techniques such as impregnation. It was observed that nanoparticles prepared by photodeposition had lower performance than impregnation method due to the relatively larger nanoparticles obtained by the former method. The best activity was attributed to the particles prepared by photodeposition at pH ~ 5.5.

Tseng and Wu [53] claimed that by changing the time of irradiation and concentration of precursor (HAuCl₄), they could achieve size-controlled Au nanoparticles on the surface of ZnO nanorods: shorter irradiation time and lower (HAuCl₄) concentration caused smaller particle sizes, though the reason behind this phenomenon was not explained. Nevertheless, the smaller particles showed better catalytic activity. Supporting this hypothesis, by increasing the size of Au nanoparticles more than 30 nm, a destructive influence on the photocatalytic activity was noticed. It was suggested that this was possibly due to the limited light scattering which was caused by large Au particles and decreased the light absorption of ZnO nanorods.

Naknam *et al.* [54] investigated the effect of light intensity on the deposition and morphology of Au nanoparticles on ZnO. It was reported that by increasing the light intensity, the illumination period was deliberately shortened to keep the number of photons required for ZnO illumination constant. The pH was fixed at 8 by using Na₂CO₃. Although the amount of nanoparticles loading and their average size were not changed, the agglomeration degree was definitely increased by increasing the light intensity.

In a different research also conducted by Naknam *et al* [54], it was stated that ZnO morphology has a significant role in the size determination of photodeposited Au nanoparticles. Compared to the Au particles deposited on small nanorods of ZnO, the particles were definitely larger when deposited on larger ZnO nanorods or microflowers. Thus, it was concluded that ZnO surface area should also be taken into account for the optimized photodeposition of Au nanoparticles.

It was discussed by Wu *et al.* [55] that Au particles photodeposition can be controlled with regards to the deposition site and content by the concentration of H₂AuCl₄ and illumination time. In two separate studies conducted by He *et al.* [56] and Su and Qin [57], the loading content of Au was changed. It was observed by He *et al.* [56] that increasing Au loading to 10 mol% enhances the photodeposition rates of salicylic acid and methylene blue.

According to all the gathered data from the literature, the best conditions to obtain small and individual nanoparticles of Au are 1) large ZnO surface area, 2) low concentration of H₂AuCl₄, 3) illumination light applied at low concentration and long time. Separately obtained small Au nanoparticles have zero oxidation state, independent of using any sacrificial agent.

Mostly used precursors for Pd photodeposition on ZnO are PdCl₂ [58-60] and H₂PdCl₄ [61]. Also, mostly utilized sacrificial agents are acetic acid [60], ethanol [59], and methanol [58]. In the work conducted by Chang *et al.* [59], Pd photodeposition on ZnO surface was carried out by using ethanol as the sacrificial agent without purging any inert gas. XPS analysis of the obtained sample showed that in addition to the observed energy peak corresponding to metallic form of Pd, another Pd 3d_{5/2} binding peak was achieved which was attributed to PdO. They claimed that no PdO peaks were observed by transmission electron microscopy (TEM) or XRD investigations. Therefore, it was concluded that the observed PdO peaks were originated from the ion-sorbed O₂ at the Pd surface. On the other hand, the nanoparticles surface oxidation is a well-known phenomenon when exposed to the atmospheric conditions for a long time. Hence, the O₂ ion-sorption is considered as the surface of PdO. In another study performed by Jin *et al.* [61], who used a different precursor with the absence of any sacrificial agent, no binding energy peak related to PdO was observed. This suggested the selective formation of metallic Pd and therefore, no oxidation happened on the PdO surface. Liqiang *et al.* [60] used both nitrogen purging and a sacrificial agent in the precursor preparation and they observed the

formation of metallic Pd. In both works conducted by Jin [61] and Linqiang [60], optimum loading of Pd were investigated. Optimal Pd loading of 0.05 mol % (0.065 wt%) on ZnO nanorods was found by Jin *et al.* [61] for the application of rhodamine B degradation. The optimal loading amount of Pd on the surface of ZnO nanoparticles achieved by Linqiang *et al.* [60] was 0.5 wt% for the application of n-C₇H₁₆ photocatalytic degradation. In conclusion, although the presence of both a sacrificial agent and inert atmosphere result in decreasing Pd particles size, it seems that the conditions of photodeposition procedure have little effects on the Pd oxidation state on ZnO surface.

Gomathiasankar *et al.* [62] investigated the photodeposition of Copper particles on the ZnO surface using methanol as the sacrificial agent. Hydrogen evolution reaction was measured in situ. A xenon lamp (500 W) was used as the illumination light source. Light intensity was set at 1.0 mW/cm² and measured in the range of 320- 410 nm. The optimal loading of 6 wt% Cu on ZnO was obtained to yield the maximum hydrogen formation. Photoluminescence studies indicated that Cu photodeposition subdued the recombination of electron and hole, suggesting that Cu acts as a trapping site for electrons.

1.5 Photodeposition of Nanoparticles on Graphene

So far, numerous researches have been dedicated to the synthesis development of metallic nanoparticles (MNPs) and their photodeposition on the surface of graphene composites [63]. Two key factors in all the performed studies is 1) uniform distribution of metallic nanoparticles and 2) decreasing the nanoparticles size. These parameters are specially considered for the applications such as catalyst preparation in which, the surface area of MNPs is very important, or for applications that require using expensive noble metals [64-66]. Two other important features to achieve an efficient synthesis method are 1) acceptable attachment of MNPs on the surface of graphene sheets and 2) the proper electrical connection between the MNPs and graphene surface [67]. In the majority of developed methods, the common solution is to reduce the metal in the solution due to the presence of graphene. The only differences are the techniques which were used for the reduction reaction. However, all the reduction reactions are either chemical (by using a reducing reagent or electrochemical (through an external power source [67]).

Chemical reduction methods are very suitable for scaling up due to their simplicity and flexibility in using different graphene composite forms such as powder or film. Moreover, The size and morphology of the MNPs are easily controllable by changing the reaction conditions e.g. reactants concentrations, time and temperature [68]. However, there are a few challenges accompanied with this method. First, changing and controlling the reduction reaction conditions are not usually sufficient enough to achieve the desired effectiveness. Second, nanoparticles reduction can happen at random points inside the suspension/solution, thus it will be hard to adequately attach the nanoparticles to the surface of graphene sheets. This problem is even more pronounced while using noble metals due to their very high cost. In contrast, much better control over the reaction conditions can be achieved by using electrochemical methods, since the electron flow from an external power source can be much more easily controlled [68]. In addition, by passing the electron current through the graphene sheet, MNPs can be properly attached by electrical forces to the graphene surface. However, the application of electrochemical methods for deposition of metal nanoparticles is limited to the graphene sheets (films) and thus, the uniform distribution of MNPs on the graphene film surface is highly dependent on the local conductivity of these films [69].

Consequently, developing a new technique to overcome the challenges of both chemical and electrochemical methods is essential. One way to solve the issue concerning local conductivity of graphene sheets is to attach various nano-electron generators (NEGs) to the different regions of the graphene surface (Figure 5a) with the ability to quickly switch them on and off when required (Figure 5b, c). Most suitable platforms for this application are functionalized graphene (FG) films with wide bandgaps. Covalent bonding between the functional groups and graphene sheets is well-known to form bandgaps at different points of the FG which can play the role of mentioned NEGs, which in turn can be immediately switched on and off by using a pulsed illumination light provided by a UV source (Figure 5b, c). By varying the illumination time on each pulse, the number of generated (photoexcited) electrons can be adjusted and as the result, the MNPs growth on the FG sheets can be precisely controlled. After successful deposition of MNPs, various chemical or thermal procedures can be applied to remove the functional groups from the FG films. Metallic nanoparticles can be deposited over a wide range of size including sub-nm clusters to nm-sized particles. The advantage of this approach is that the reduction of MNPs is only limited to the graphene sheets and not at random points inside the suspension/solution. Also, electrical connection between the nanoparticles and graphene

surface is guaranteed. Moreover, due to the homogeneous distribution of functional groups, which has been shown in this work, photodeposited nanoparticles are also uniformly distributed over the graphene sheets [70].

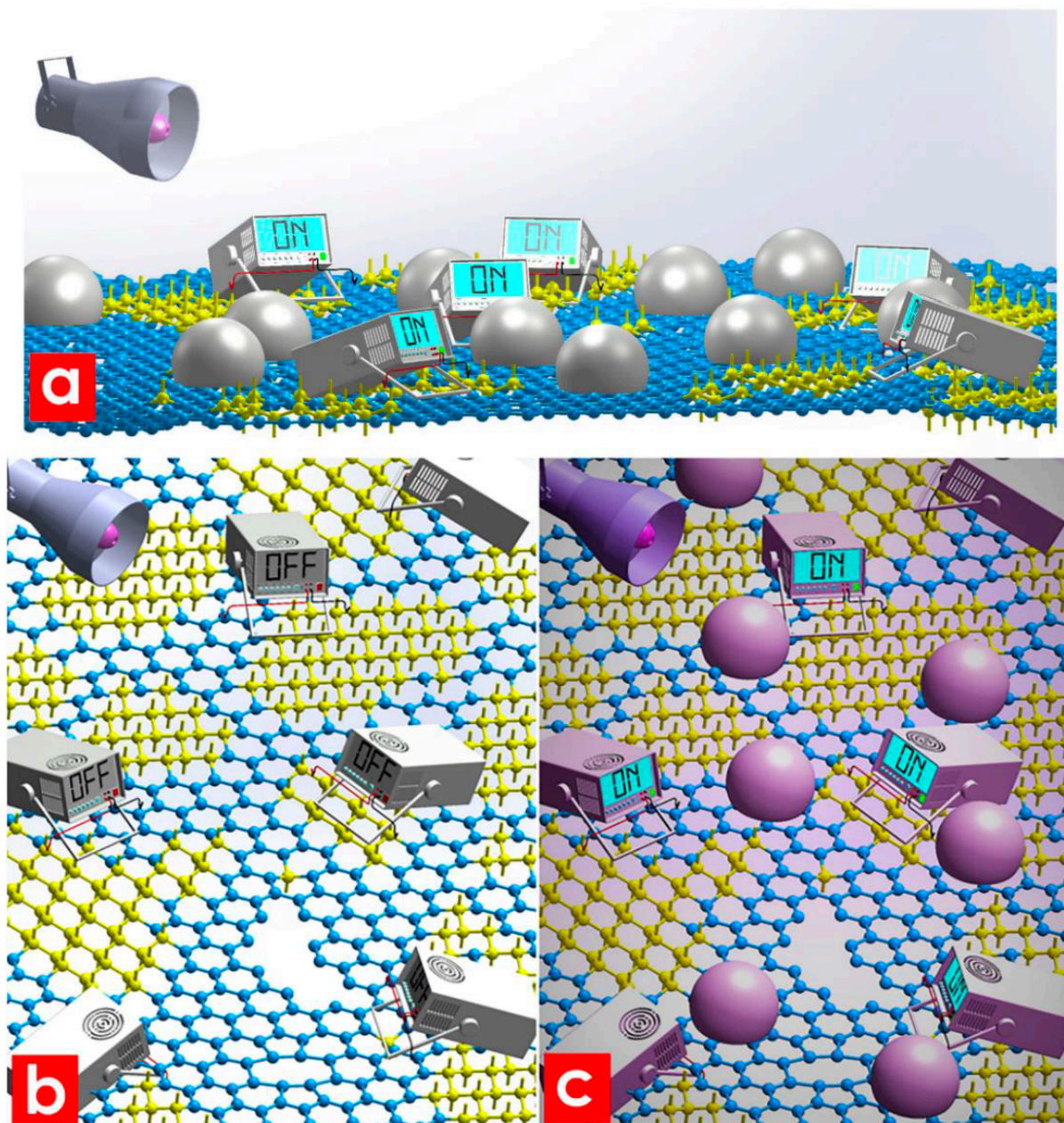


Figure 5. Schematically illustration of (a) functionalized graphene, NEG-decorated; (b) when all NEGs are off, dark mode; (c) NEG-decorated (functionalized) graphene under UV illumination, starting point of Pt nanoparticles growth. The yellow and blue colored atoms have hybridizations of sp^3 and sp^2 , respectively.

1.6 Nanoparticles Photodeposition on Other Metal Oxides

1.6.1 Gallium Oxide

In spite of having quite considerable band gap, 4.5 eV, Maeda *et al.* [71] and Busser *et al.*, [14, 72] studied photodeposition behavior of Ga₂O₃, because of favorable photocatalyst characteristic of (Ga_{1-x}Zn_x) (N_{1-x}O_x) compound. In the work has been done by Maeda *et al.* [71], Rh_{2-y}Cr_yO₃ was photodeposited on β-Ga₂O₃ by means of irradiation of the solution bath with the composition of (NH₄) RhCl₆, and K₂CrO₄ without using sacrificial agent under inert gas atmosphere for period of 4 hours. They showed that the composite product, Rh_{2-y}Cr_yO₃/β-Ga₂O₃, has 10 times more activity in photocatalytic water splitting compared to β-Ga₂O. In the other work has been done by Busser *et al.* [14], they fabricate core shell structure through double step photodeposition of Rh/Cr₂O₃ on Zn-Ga₂O₃. They used methanol as sacrificial agent in aqueous solution under inert gas atmosphere of N₂. The photodeposition process with Hg lamp at 350 W was started after adding 0.025 wt. % Rh from Na₃RhCl₆·3H₂O. The photoreduction of Rh³⁺ to Rh⁰ was succeed through the following reduction equation.



They measured in-situ H₂ evolution rate as a result of sacrificial agent's (methanol) reformation to find optimum concentration of Rh source. As shown in Figure 6, they added different amounts of Na₃RhCl₆·3H₂O intervalley, by switching on/off the illumination, in order to find optimized amount of Rh loading (0.1 wt.%).

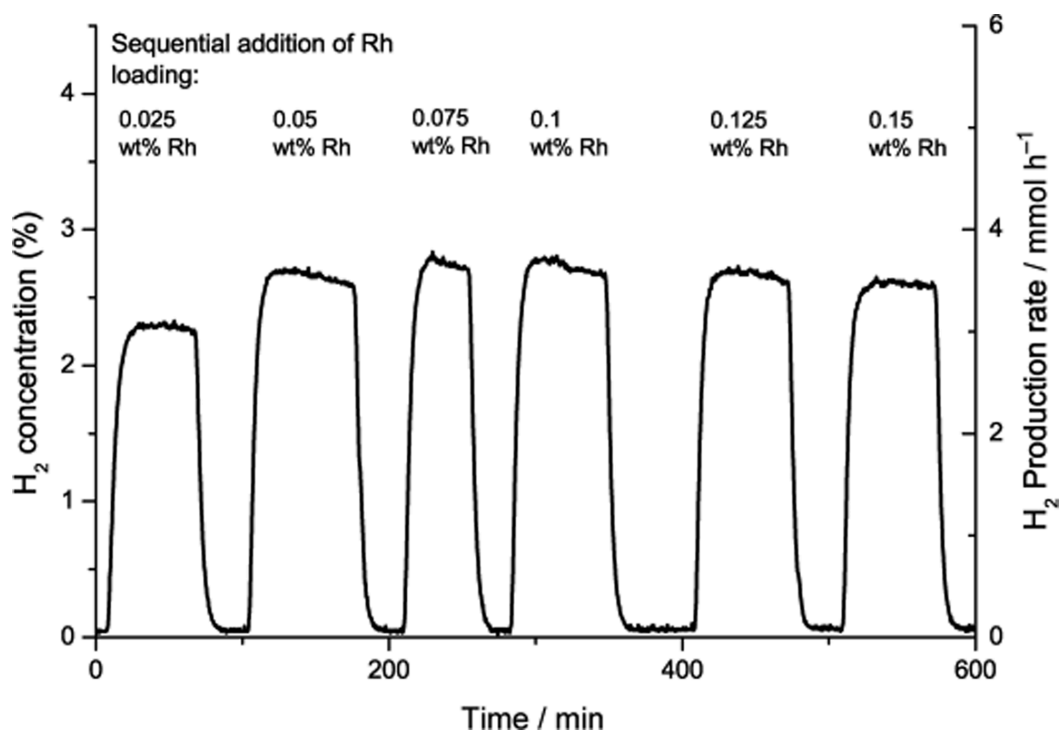
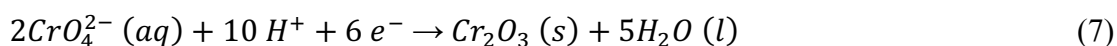


Figure 6. in-situ measurement of H₂ production while the photodeposition of Rh on Zn-loaded Ga₂O₃ [14].

Identical step-by-step photodeposition procedure was carried out to acquire photodeposited Rh/Cr₂O₃ particles on Zn-loaded Ga₂O₃. In this time, they found out 0.09 wt.% concentration as an optimized value for Cr₂O₃. The photoreduction of Cr₂O₃ as a shell layer was proposed as the following equation.



By found optimized concentration of both Rh and Cr₂O₃ loading, the authors showed the considerable difference in H₂ evolution between step-wise photodeposition of Rh/ Cr₂O₃ nanoparticles and simultaneously version. photodeposition of Rh/ Cr₂O₃ showed higher rate of H₂ production compared to the latest. In the other work of Busser *et al.* [72], they photodeposited CuO_x and Cr₂O₃ in two steps on β-Ga₂O₃ by using the same reactor setup, as mentioned before.

The size of photodeposited nanoparticles of CuO_x on was determined 1-10 nm which small size range of nanoparticles were attributed to Cu₂O and the larger size range of nanoparticles were corresponded to Cu phase. They confirmed the Cu formation by XPS as shown in Figure 7.

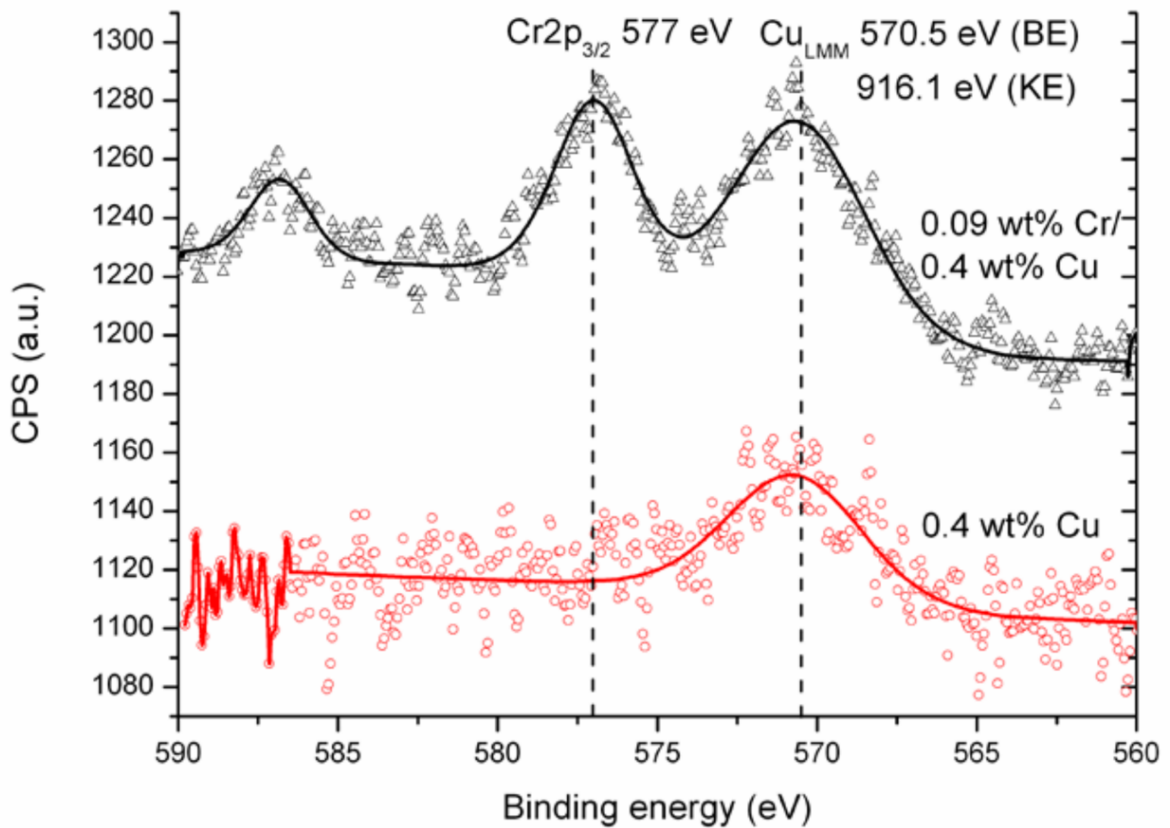


Figure 7. Characteristic XPS spectrum of the Cr 2p and the Cu_{LMM} Auger region of the samples of 0.4 wt% Cu on Ga₂O₃ and 0.09 wt% Cr 0.4 wt% Cu on Ga₂O₃ [72].

1.6.2 Bismuth Vanadate, BiVO₄

Due to having narrow band gap of Bismuth vanadate (2.3–2.9 eV), it is considered as a promising photocatalyst material for oxygen evolution in order to water splitting under illumination of visible light spectrum, both in Zscheme configuration and the presence of sacrificial agent [73-76]. The common used sacrificial agent for this photocatalyst material is AgNO₃ [73-76]. Zhang *et al.* [77] produced photodeposited Ag/BiVO₄ film with the nanoparticles size range 10-20 nm for Ag. The photodeposited Ag nanoparticles promoted the BiVO₄'s catalytic activity in the application of phenol degradation under visible light waves. Similar to the former research, Kohtani *et al.* [78] investigated the phenol degradation under visible light waves by means of Ag/BiVO₄ nano-composite, however they used two methods of impregnation and photodeposition with different concentrations. (1.3 wt % Ag and 2 wt % Ag, respectfully). Enhanced photocatalytic activity of BiVO₄ by means of Ag nanoparticle deposition was proved again. However, they showed considerable enhancement of photocatalytic activity of nanocomposite of Ag/BiVO₄ by impregnation compared to photodeposition. In figure 8, by using Auger electron spectra, they showed that enhancement

of photocatalytic activity of nanocomposite of Ag/BiVO₄ by impregnation is correlated to presence of oxide form of Ag (Ag₂O or/and AgO).

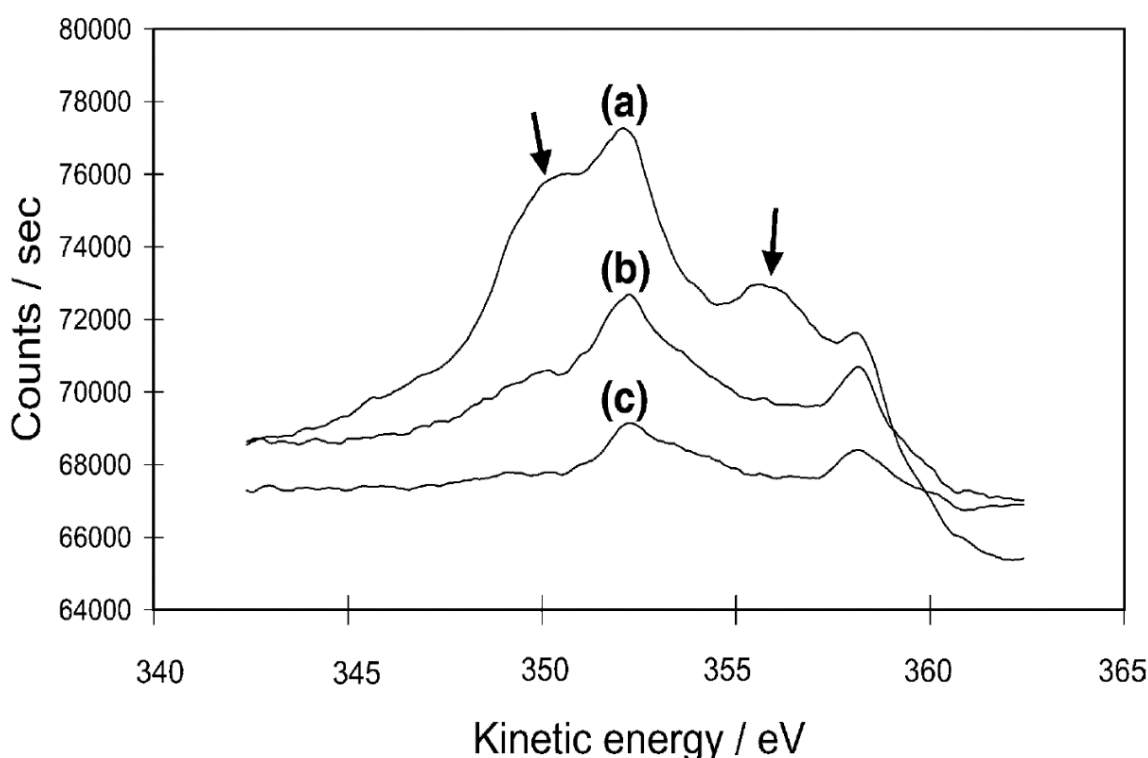


Figure 8. Auger electron spectrum of different concentration of Ag/BiVO₄ by impregnation and photodeposition. a) 1.3 wt.% Ag/BiVO₄ by impregnation. b) 1.3 wt.% Ag/BiVO₄ by impregnation in the exposure of H₂ stream for 1 hr at 353 K. c) 2 wt.% Ag/BiVO₄ by photodeposition [78].

They proposed that the Ag oxide species were detected on the surface of Ag nanoparticles. The both oxide form of AG, AgO and Ag₂O, were not found in photodeposition method. For the mechanism of enhanced catalytic activity of Ag/BiVO₄ by impregnation, they proposed that adsorption of phenol molecules on the surface of oxide form of AG, AgO and Ag₂O, were favorable. Due to large size range of Ag nanoparticles in impregnation method, FE-SEM characterization method was used for impregnation, however it was not possible to detect the nanoparticles produced by photodeposition owing to small size range, *i.e.*, by using photodeposition method, the size range and nanoparticle distribution of Ag are smaller than impregnation. In both studies of Kohtani *et al.* [78] and Zhang *et al.* [77], neutral gases atmosphere and sacrificial agent were not utilized during photodeposition process.

1.6.3 Tantalum Oxide, Ta₂O₅

Similar to previous mentioned photocatalyst material, Gallium Oxide, Ta₂O₅ has also wide band gap of 4.0 eV [79-81]. Zhou *et al.* [79] showed that by plasmonic photodeposition of gold over mesoporous phase of Ta₂O₅, considerable photocatalytic activity under visible light waves can be obtained. In figure 9, they showed photodecomposition behavior of RhB in aqueous media with and without Au nanoparticles. They photodeposited the Au by using HAuCl₄ as a precursor, methanol as a sacrificial agent, and the room temperature was kept by using water bath, under inert N₂ gas atmosphere. For reformation of methanol producing hydrogen, they noted 1.0 wt % Au as the optimized concentration. They controlled the size range of photodeposited Au nanoparticles by adjusting different illumination time, 10 min, 60 min, and 120 min for achieving 10 nm, 15 nm, and 20 nm nanoparticle size. They showed that higher photocatalytic hydrogen production of methanol, $\lambda > 400$ nm, was due to large nanoparticle sizes. They correlated the high photocatalytic production of methanol due to large nanoparticle with surface plasmon resonance (SPR) effect.

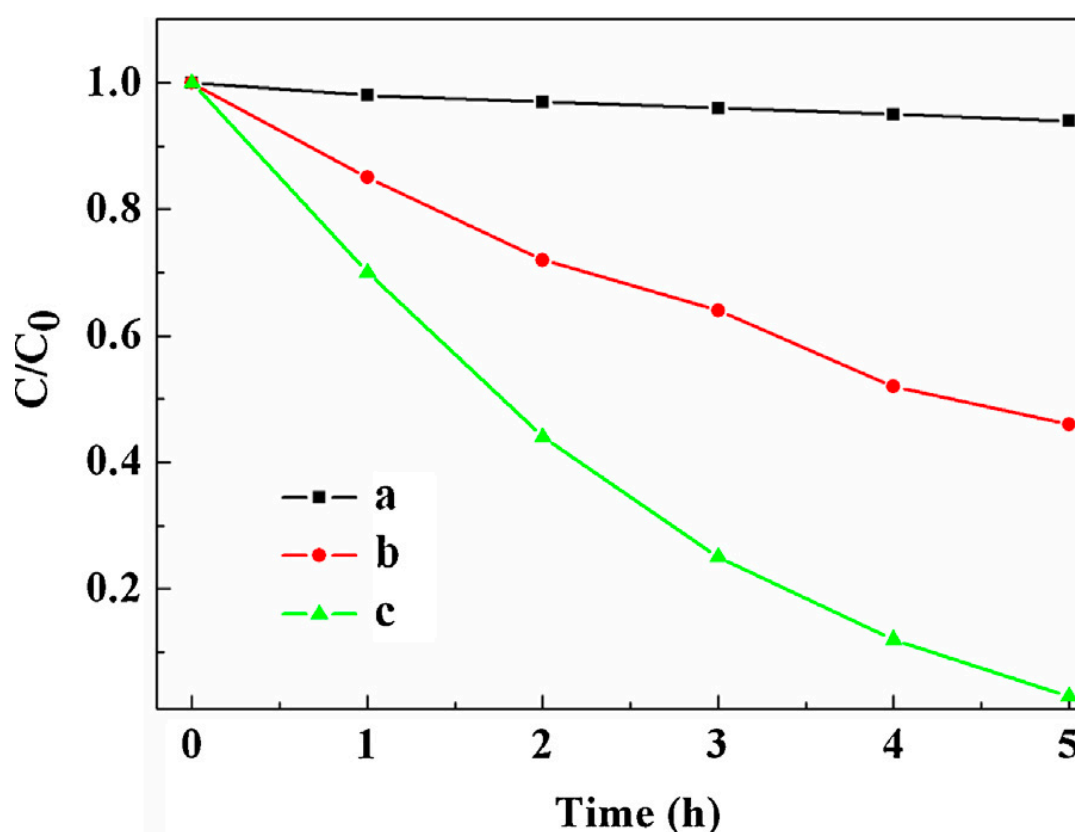


Figure 9. Photodecomposition behavior of RhB in aqueous media with and without Au nanoparticles, a) without photocatalyst, b) 1.0 wt% of Au-Ta₂O₅ c) 1.0 wt% of Au-Ta₂O₅ under visible light illumination [79].

1.6.4 Strontium Titanate, SrTiO₃

Another mostly known photocatalysts is SrTiO₃ that have a quite large band gap of 3.2 eV [3]. However, many researches addressed the wide band gap by introducing dopant elements in the crystal lattice such as chromium [82, 83], rhodium [76, 84], and niobium [85, 86]. Platinum is the most used element for photodeposition of doped SrTiO₃.

In different works done by Sasaki *et al.* [87], Lee *et al.* [88], and Yu *et al.* [76], they photodeposited Pt on doped Rh:SrTiO₃. However, they found different forms of Pt, metallic Pt and oxide form of Pt. Sasaki *et al.* [87] demonstrated photodeposition metallic Pt on the substrate with the inert N₂ gas atmosphere with using sacrificial agent, though Lee *et al.* [88] showed oxide form of Pt after postdeposition process without using inert gas neither sacrificial agent. Surprisingly, Yu *et al.* [76], found both metallic Pt and platinum oxide form after postdeposition process without using inert gas neither sacrificial agent. In addition to Pt photodeposition on doped SrTiO₃ substrate, some researchers have done photodeposition of silver on doped SrTiO₃ substrate [89, 90].

In order to achieve Ag photodeposited nanoparticles on SrTiO₃ nanotube substrate, Sun *et al.* [90] studied two photodeposition processes. First, they investigated about classical method for photodeposition for 180 min, without using sacrificial agent in AgNO₃ containing bath. Then, after immersion of SrTiO₃ nanotube substrate in AgNO₃ containing bath for 24 h at the temperature of 60 °C, they started illumination in presence of methanol as a sacrificial agent for 60 min. As the result of first method, they did not find any Ag nanoparticles deposited on the substrate, however, Ag nanoparticles were found in second method. They demonstrated metallic Ag nanoparticles by mean of XPS, as figure 10. They noted that photocatalytic activity of produced nanocomposite for degradation of methyl orange was increased.

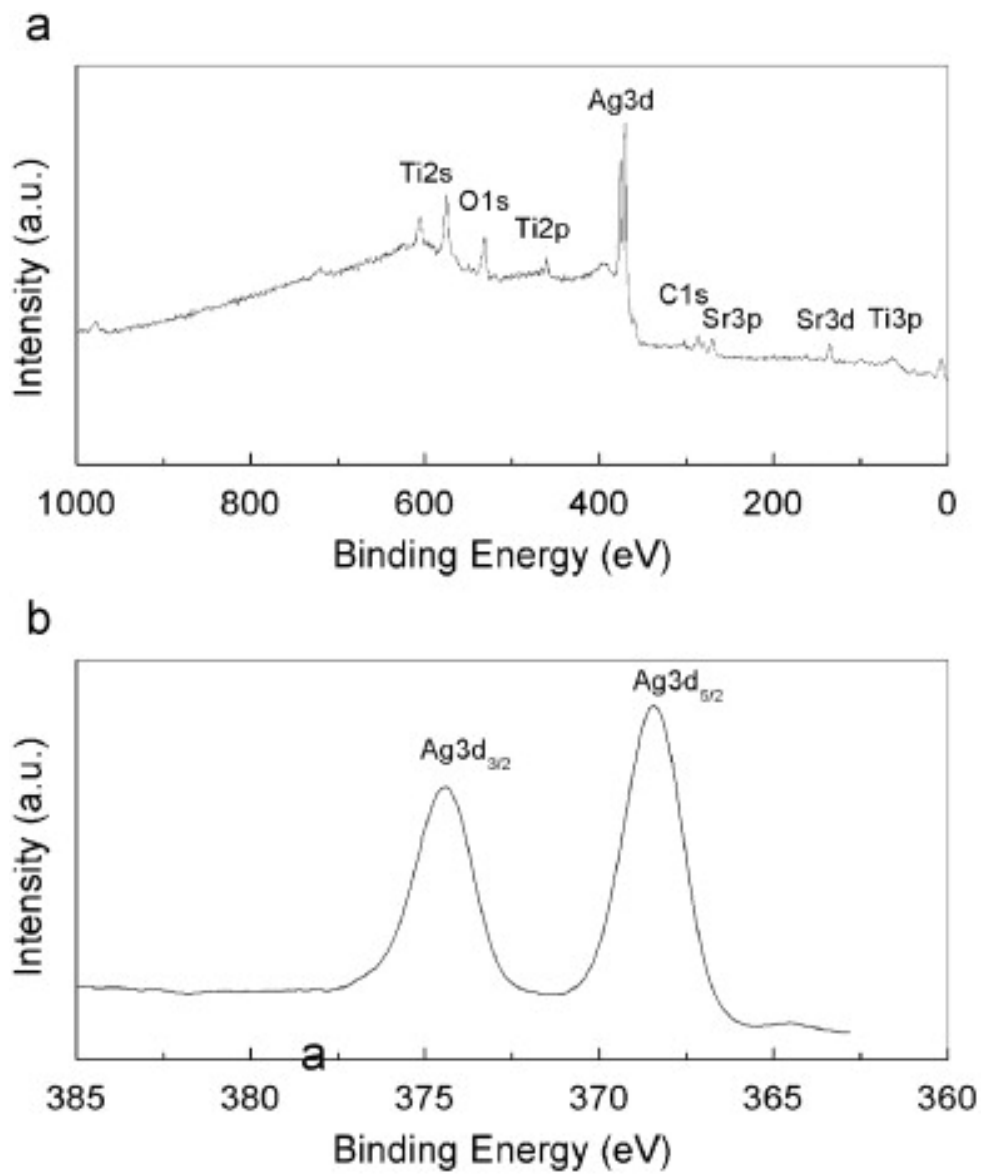


Figure 10. X-ray photoelectron spectrum of Ag nanoparticles photodeposited on SrTiO₃ nanotube substrate. a) wide scan spectrum b) Deconvoluted spectra for Ag 3d [90].

Objective of This Work

2 Objective of This Work

The main objective of this work was development of the novel continuous-flow photodeposition reactor by monodisperse and uniform photodeposition of different noble metal nano-particles on various photocatalyst materials. During the project, the following features were aimed to achieved:

- Up-scalability;
- Simplicity yet novel;
- Cost-effectivity;
- Precise monodispersion and uniform distribution of the noble metallic nanoparticles;

In addition, applicability of photodeposition of different noble metal nano-particles (platinum, and gold) on various photocatalyst materials (TiO_2 , and PRGO).

Materials and Methods

3 Materials and Methods

3.1 Design of Photocatalytic Deposition Reactor

As schematically Figure 11 illustrates the full setup of the novel photocatalytic deposition reactor, the interior surface of a polyvinyl chloride tube (length x diameter = 55 cm x 15 cm; other types of materials can also be employed) is covered by mechanically polished, thick, and sticky back foil of Aluminum. The sticky back Aluminum foil acts as a UV reflector layer which does not let the UV illumination efficiency drop. As a UV illumination source, five UV-C lamps with 55W power (Philips TUV PL-L 55W/4P HF 1CT/25) was installed inside the polyvinyl chloride cylinder with having equal distances from each other. To provide a path for continues flow of the solution with concentric configuration inside the polyvinyl chloride pipe, a quartz tube (length x diameter = 55 cm x 0.5 cm) was fixed vertically along the central axis of polyvinyl chloride pipe. To prevent any possible high temperature effect of the system by UV illumination lamps on kinetics of the deposition reactions during the continuous photodeposition operation, a heavy-duty cooling fan was used at the ending point of the polyvinyl chloride pipe to cool down the whole chamber. In addition, an ice-water bath was used to control the temperature of suspension. Temperature of the suspensions was checked before and after the UV illumination which never surpassed 3°C and 7°C, respectively. To make a continuous flow of the suspension through the quartz tube fixed in the center of the chamber, a magnetic pump with a circulation rate of 16 L.min⁻¹ is used. It is noteworthy to mention that the gravitational forces applied on the liquid effects on the flow rate of suspension's circulation, hence all parts of the reactor were fixed firmly. In view of the fact that any change (vertical displacements) in the configuration of the reactor causes flow rate deviation. The quartz tube was covered with the same sticky back aluminum foil selectively. To open specific window length for the pulsed excitation of UV illumination, the coverage was 5cm x 2cm.

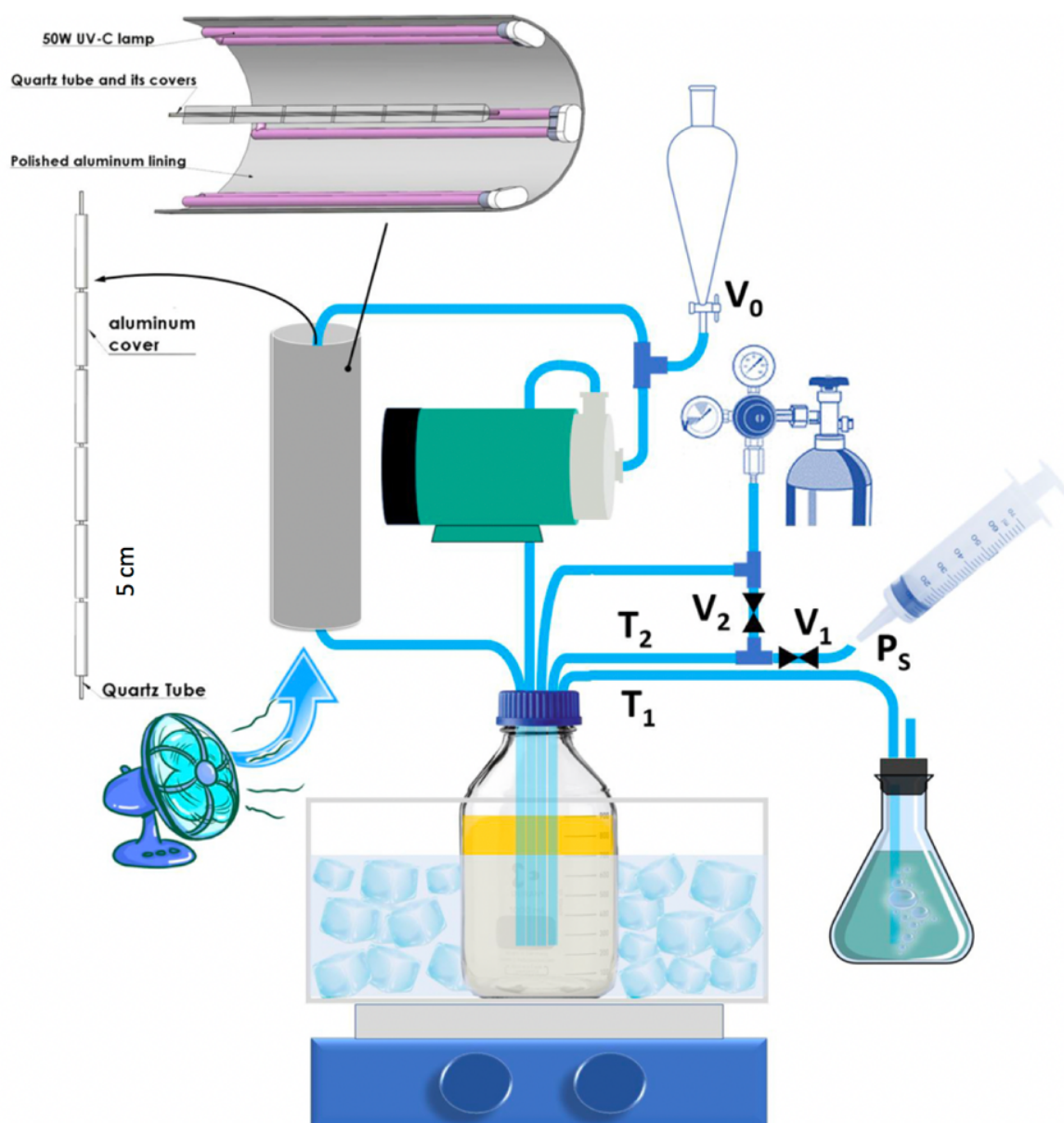


Figure 11. Schematically detailed illustration of the photocatalytic deposition reactor. The N_2 gas outlet from the suspension is conducted to the bubbler through T_1 pipe. The P_s point is the sample collection point in different times (the ending point of T_2 tube). V_0 , V_1 , and V_2 are the valves for initial feeding, sampling and tube evacuation, respectively [91].

3.2 Supplying the Reactants to the Continuous-flow Photodeposition Reactor

Reactants were filled into the separation funnel which was located in higher vertical position than the reservoir and the magnetic pump. To operate well, the location of the pump should be in high vertical level compared to the reservoir's bottom. In order to feed the reactants to the reactors, V_0 valve was opened and to avoid entering air to the liquid flow, the V_0 valve should be closed when the reactants in the funnel just depleted.

3.3 Synthesis Procedures

3.3.1 Synthesis of GO

To produce the PRGO, firstly the synthesis of GO was done according to optimized version of Hummers. 100 mL of sulfuric acid (98%, H₂SO₄, Sigma Aldrich) and 2 g of graphite (>99%, Sigma Aldrich) were added in a 500 mL Vol. Erlenmeyer flask. The temperature of the mixture was fixed ~0 °C by using ice-water bath while mechanically mixing the content by a magnetic stirrer. Due to high viscosity of the suspension after completing the reaction, a big slide-round magnetic bar was used. Adding 6 gr of potassium permanganate was done gradually in 30 min since the reaction is very exothermic and afterward continued for 6 h without ice-water bath. Then, 250 ml of deionized water was added dropwise, by using a separation funnel, while the suspension's temperature was kept ~ 0° C in ice-water bath. Later on, 30 mL of hydrogen peroxide (H₂O₂) was added gradually on the magnetic stirrer, without having ice-water bath. To obtain desired material with pH of 5, washing process with deionized water was done by centrifugation of the suspension, for 15min at 3500 x g, for several times. In each step of the centrifugation process, the supernatant was discarded and the precipitation was washed with deionized water. Then the obtained material was added to 500 mL of 1 M hydrochloric acid and stirred for 1 h. Again, abovementioned washing process with the centrifugation method was applied to reach pH 5. The obtained material from the previous step was added to 1 L of deionized water and was sonicated in an ice-water bath sonicator for 3. As a final purification step, the product was centrifuged for 3 times of 20 min at 3,500 x g and, each step, the precipitation was discarded. Solid content of obtained GO suspension was determined by drying the suspension in oven and weighing, consequently. To store the diluted GO suspension in a capped amber bottle, the concentration of the suspension was adjusted to 0.2 g/L by adding required amount of deionized water

3.3.2 Synthesis of Partially Reduced GO (PRGO)

To prepare the PRGO from GO, diluted GO with a concentration of 0.2 g/L was added gradually in a round bottom flask having an equal amount of a 4 M sodium hydroxide inside. Then a condenser was attached to a flux and the reflux-stir of the suspension was kept at 90 °C for 8 h by using a heating mantle. Finally, after cooling down the suspension, like abovementioned purification process by centrifugation, the precipitate was washed by deionized water to reach near neutral pH.

3.3.3 Photocatalytic Deposition of Platinum on PRGO

To travel the UV light's illumination through the suspension easily, the concentration of 50 mg/L of PRGO in deionized water was fixed. The diluted suspension of PRGO in deionized water was probe sonicated for 1h in an ice-water bath. After getting well distribution of PRGO in water by probe sonication 60 mL of ethanol as a hole scavenger was added in 540 mL of PRGO-water suspension and kept for an hour in ice-water bath sonication. To prepare a 20 wt% Pt/graphene composite, 169 μ L of commercial 8 wt% hexachloroplatinic acid aqueous solution was added to the suspension and stirred for 20 min in room temperature. To flush out the dissolved oxygen gas of the suspension and cool down the suspension, the N₂ gas with high flow was injected for 30 min. The gas outlet tube (T₁ in figure 11) was put and fixed in a Erlenmeyer flask which filled ~0.7 L of water to conduct gas bubbles out of the system. Then the magnetic pump was started and circulation of suspension through the illumination chamber was taken place. Finally, the N₂ gas flow was reduced to have a stable circulation and the UV lights was turned on. To see the illumination time's effect on photodeposition process, sampling from the suspension was taken and washed with deionized water immediately by centrifugation.

3.3.4 Photocatalytic Deposition of Platinum/Gold on TiO₂

200 mg of commercial TiO₂ nanoparticles and 30 mL of Ethanol as a hole scavenger were added to 570 mL deionized water and the suspension was probe sonicated in an ice water bath for 1h. For different concentrations of platinum and gold, various calculated amounts of commercially available source aqueous solutions, hexachloroplatinic acid aqueous solution and hydrogen tetrachloroaurate(III) aqueous solution were added to dispersed suspension and stirred in room temperature for 20 min. To start the photodeposition process, all the practical steps for photodeposition (after suspension preparation) are the same as the photocatalytic deposition of platinum on PRGO (part 3.3.3).

3.4 Samples Characterization Methods

For morphological study of nano-particles and size distribution of the photodeposited particles, Field Emission Scanning Electron Microscopy (FE-SEM), Gemini 35 VP, and a FEI Tecnai 20 Transmission Electron Microscopy (TEM) equipped with a field emission gun were used. To prepare the samples for TEM imaging, firstly, the collected photodeposited particles was dispersed in deionized water in a very low concentration, then diluted suspension was dropped onto TEM grid. To analyse the residual cation concentration of supernatants, inductively

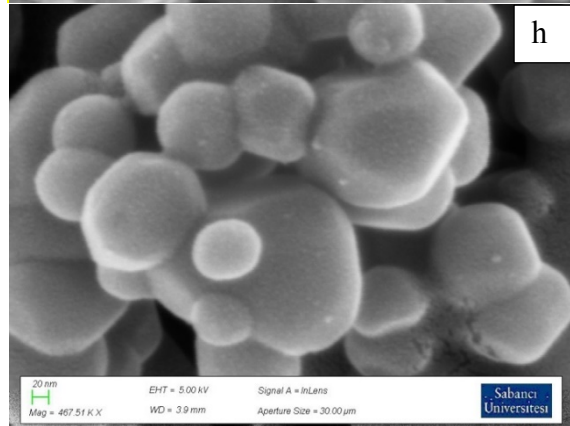
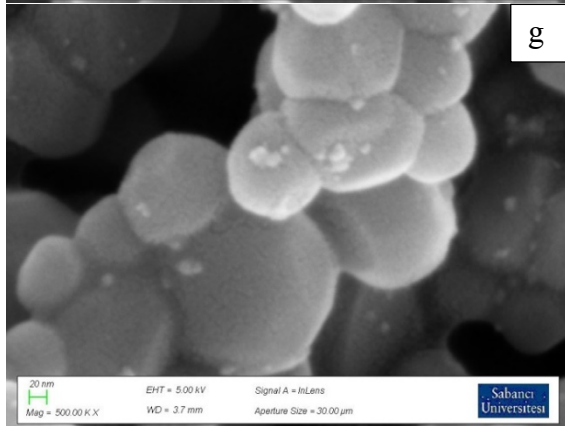
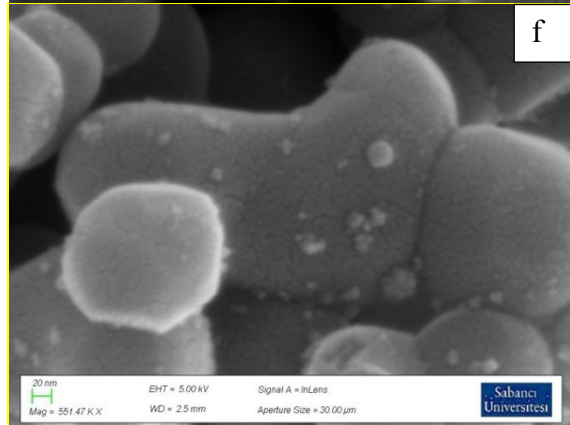
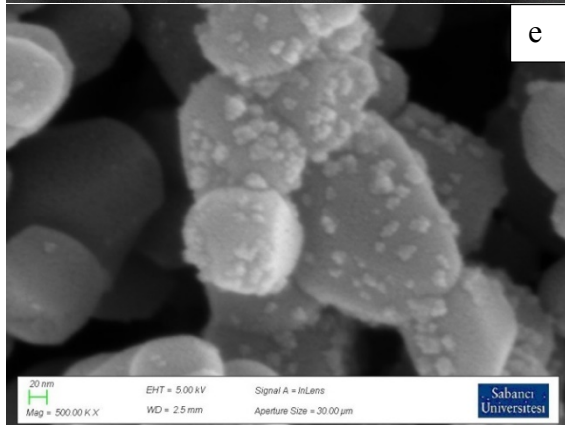
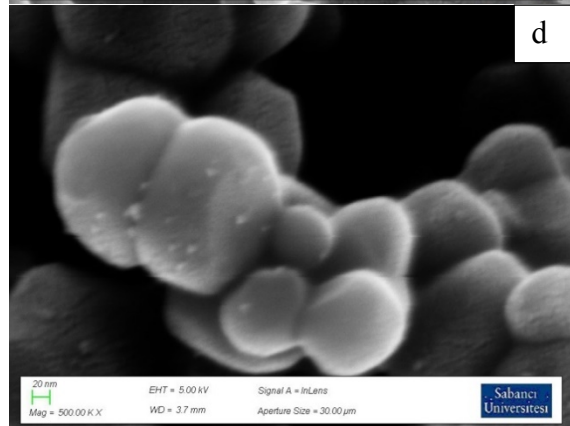
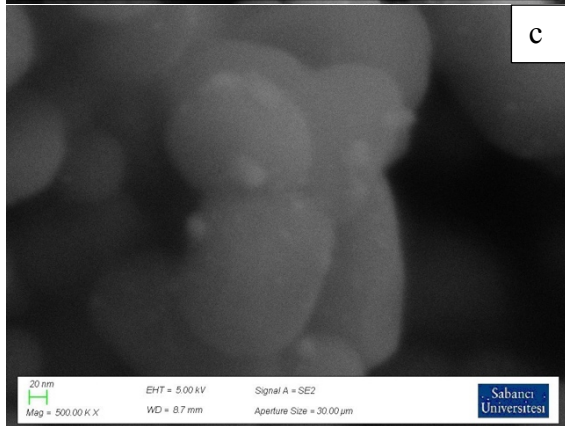
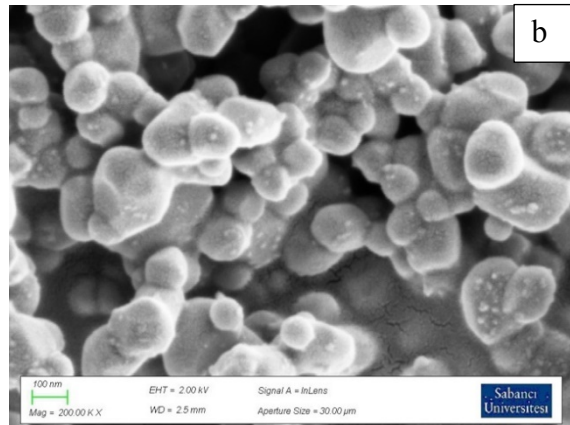
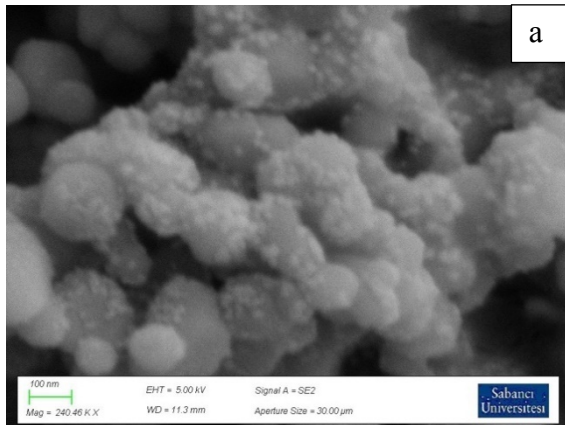
coupled plasma optical emission spectrometry (ICP-OES) was used. For compositional and phase study of photodeposited materials, X-ray photoelectron spectroscopy (XPS) were used.

Results and Discussion

4 Results and discussion

4.1 Morphological Investigation by Field-Emission Scanning Electron Microscopy

Field-emission scanning microscopy was used for morphological investigation of photodeposited nano-composites. Since the aim of this research is precise deposition of uniform monodisperse deposition of nanometallic particles over the substrates, literally, it is not feasible to see the monodisperse particles which are dispersed uniformly by means of FE-SEM. However, morphological study by FE-SEM can be helpful to narrow the focus to concentrate on the optimized parameters such as salt/substrate concentration, and illumination dose per exposure (IDE). Based on the findings from a work of our group, exposure window length for UV illumination was optimized by Abdolhosseinzadeh *et al.* [70] They used three different exposure lengths for quartz tube (4%, 20%, and 100%) for UV illumination and they found that in 20% exposure length, a precise controllable photodeposition of Pt over PRGO can be achieved. In figure 12, FE-SEM images of untreated TiO₂, nanocomposites of Pt/TiO₂, and Au/TiO₂ with different concentration ratio of noble metal to substrate were presented.



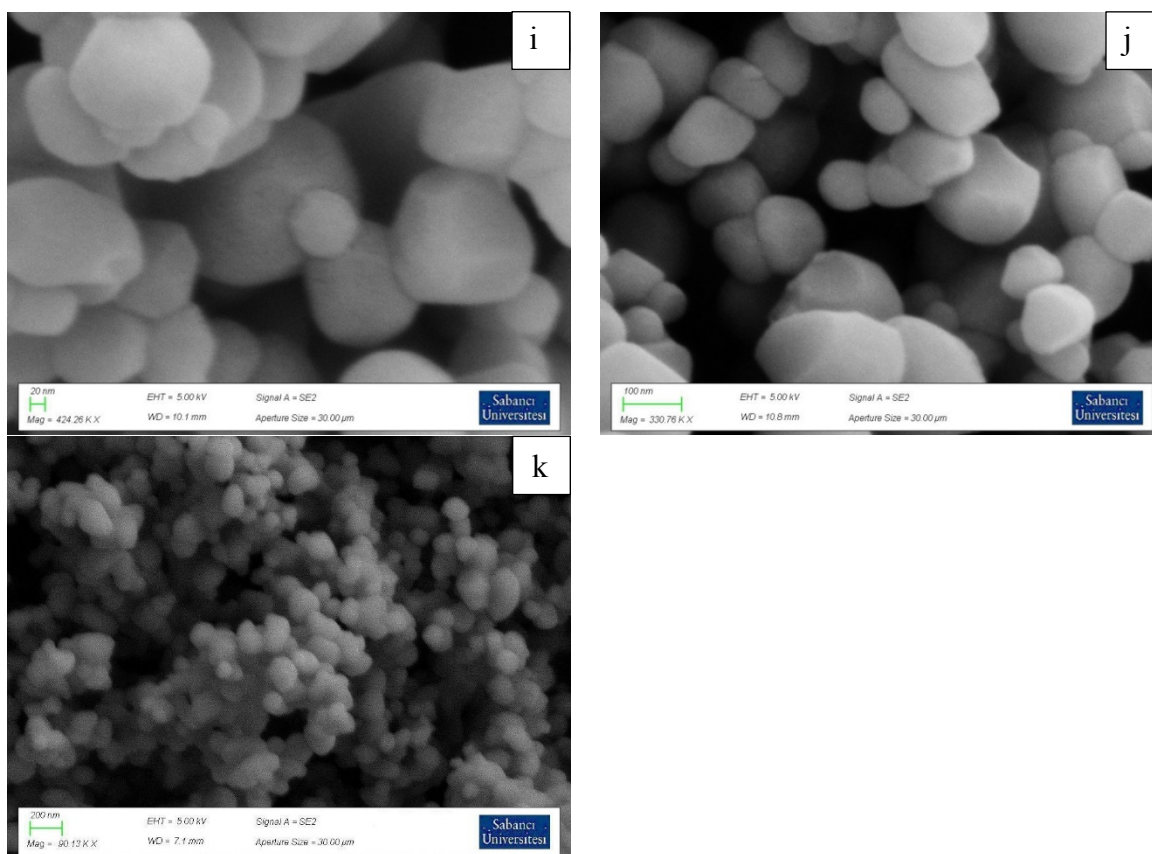


Figure 12. FE-SEM images of photodeposited catalytic nano-composites with 20% exposure length with different concentration ratio of noble metal over substrate, **a)** 7% wt. Au/TiO₂ with 4 UV lamps **b)** 7% wt. Au/TiO₂ with 2 UV lamps **c)** 5% wt. Au/TiO₂ with 4 UV lamps **d)** 5% wt. Au/TiO₂ with 2 UV lamps **e)** 7% wt. Pt/TiO₂ with 4 UV lamps **f)** 7% wt. Pt/TiO₂ with 2 UV lamps **g)** 5% wt. Pt/TiO₂ with 4 UV lamps **h)** 5% wt. Pt/TiO₂ with 2 UV lamps **i)** 2% wt. Au/TiO₂ with 2 UV lamps **j)** 2% wt. Pt/TiO₂ with 2 UV lamps **k)** untreated TiO₂.

By adding 7% wt. Au/TiO₂ in 570 mL deionized water, undesired agglomeration of Au over TiO₂ was formed. Because of a high amount of noble metal source to substrate, in both 4 UV lamps and 2 UV lamps large agglomerated precipitates were reduced on TiO₂, Figure 12 (a, b). Hence, the amount of noble metal source to substrate was decreased to 5% wt. Again, due to high amount of Au cations in the solution, agglomeration was taken place immediately after nucleation, Figure 12 (c, d). As an expected behavior, by decreasing the Au/TiO₂ ratio to 2%wt., Au precipitate was disappeared, Figure 12 (i). Therefore, the sample with the Au/TiO₂ concentration ratio of 2% wt. is the possible case for the uniform and monodispersed distribution of noble metallic particles over TiO₂ surface. Despite the fact that for reduction of Pt⁴⁺ to Pt⁰ and Au³⁺ to Au⁰, Pt needs one more electron than Au, similarly, 7% wt. and 5% wt. concentration ratio of Pt/TiO₂ showed big agglomerated noble metallic nanoparticles, Figure

12 (e-h). Identically, the sample with the Pt/TiO₂ concentration ratio of 2% wt. is the possible case for the uniform and monodispersed distribution of Pt nano particles over TiO₂ surface.

4.2 X-ray diffraction for Reduction Confirmation

In figure 13, hybrid characteristic of PRGO, representing combined both graphite and graphene oxide characteristics, by X-ray diffraction (XRD) analysis was shown. In first XRD pattern, Graphite at $2\theta=26.4^\circ$ represents a sharp peak that is indicated to 3.37 Å interlayer distance according to the Bragg's equation. Owing to Oxygen functionalized groups attachments, graphene oxide showed very sharp peak at $2\theta=8.45^\circ$, representing the considerable increased interlayer distance to ~10 Å. However, PRGO with a hybrid behavior showed both crystalline and amorphous characteristics. Due to partial de-oxygenizing of graphene oxide, according to XRD pattern, in crystalline part the interlayer spacing decreased to ~7.3 Å at $2\theta=12^\circ$. In addition, in amorphous part reduced graphene oxide behavior was shown at $2\theta=25^\circ$.

In Figure 14, X-ray diffraction patterns of PtRGO 120-60%, PtRGO 120-20%, and AuRGO confirmed the deposition of noble metals on reduced graphene oxide substrate.

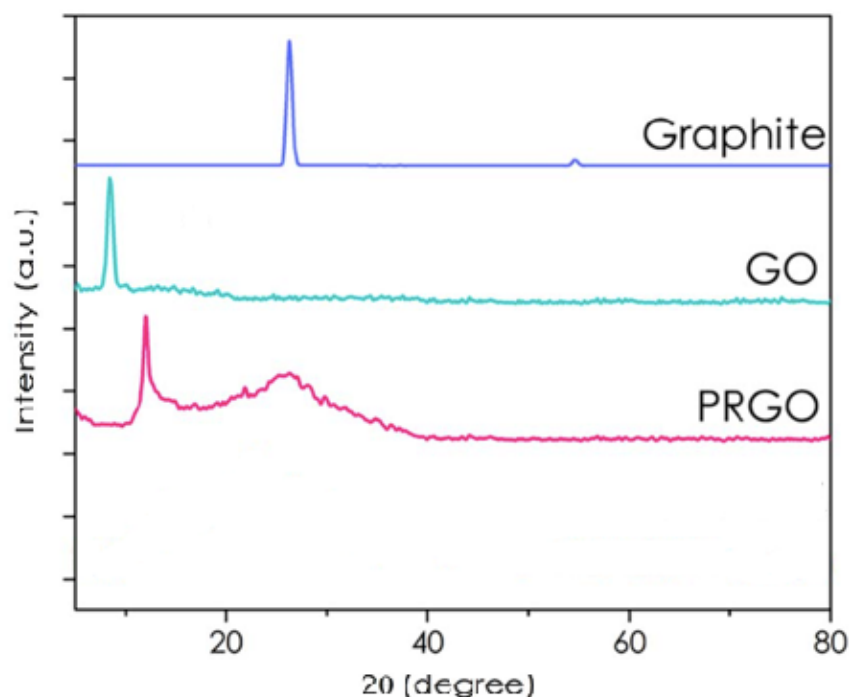


Figure 13. X-ray diffraction patterns of graphite, graphene oxide, and partially reduced graphene oxide.

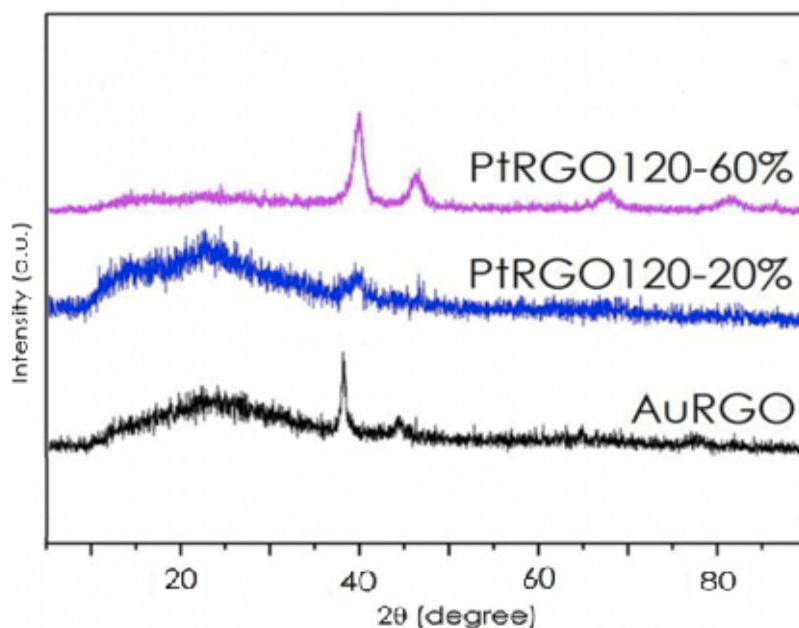


Figure 14. X-ray diffraction patterns of Pt-reduced graphene oxide 120-60%, Pt-reduced graphene oxide 120-20%, and Au-reduced graphene oxide.

4.3 Surface area and pore size analyses of Anatase TiO₂

Specific surface area and pore size distribution was investigated by Nova e-series surface area and pore size analyzer from Quantachrome Instruments as seen in figure 15. Anatase TiO₂ powders were degassed at 130 °C for 25 hours to purify all outer gas content and sample were place in liquid nitrogen (77 K) during the measurement.



Figure 15. Nova e-series surface area and pore size analyzer from Quantachrome Instruments.

The specific surface area for anatase TiO₂ were measured as 13 m² g⁻¹ and a total pore volume of 0.06 cm³ g⁻¹. Anatase TiO₂ showed type II adsorption isotherms with distinct hysteresis loops. The BJH pore size distribution curves of anatase TiO₂ demonstrated mainly mesoporous profile however it also showed a small partition of microporous distribution as well. Pore size distribution profile showed 12.7 Å as the sharpest peak and the pore sizes have a range between 10 to 50 Å as seen in figure 16.

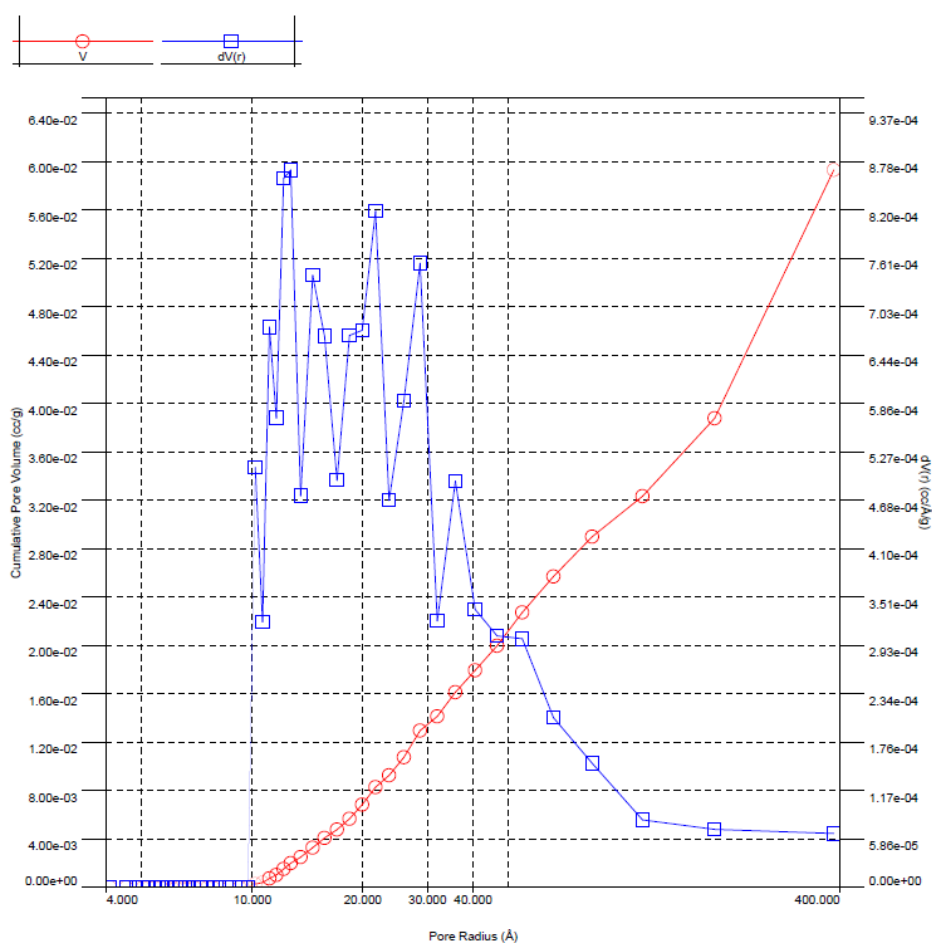


Figure 16. Pore size distributions of Anatase TiO₂ by using BJH method

4.4 Transmission Electron Microscopy for Size Distribution and Morphology

The distribution of the nanoparticles and their morphologies, which have significant effect on the performance of nanocomposite catalysts, have been studied by TEM. These two characteristics are affected by numerous synthesis parameters, but in this work, through the optimization of the illumination dose per exposure (IDE), we have been able to obtain a fairly

monodisperse and uniformly distributed noble nanoparticles on TiO₂ substrates. In figure 17, size distribution and morphology of the both Au and Pt noble nanoparticles over TiO₂ and reduced graphene oxide.

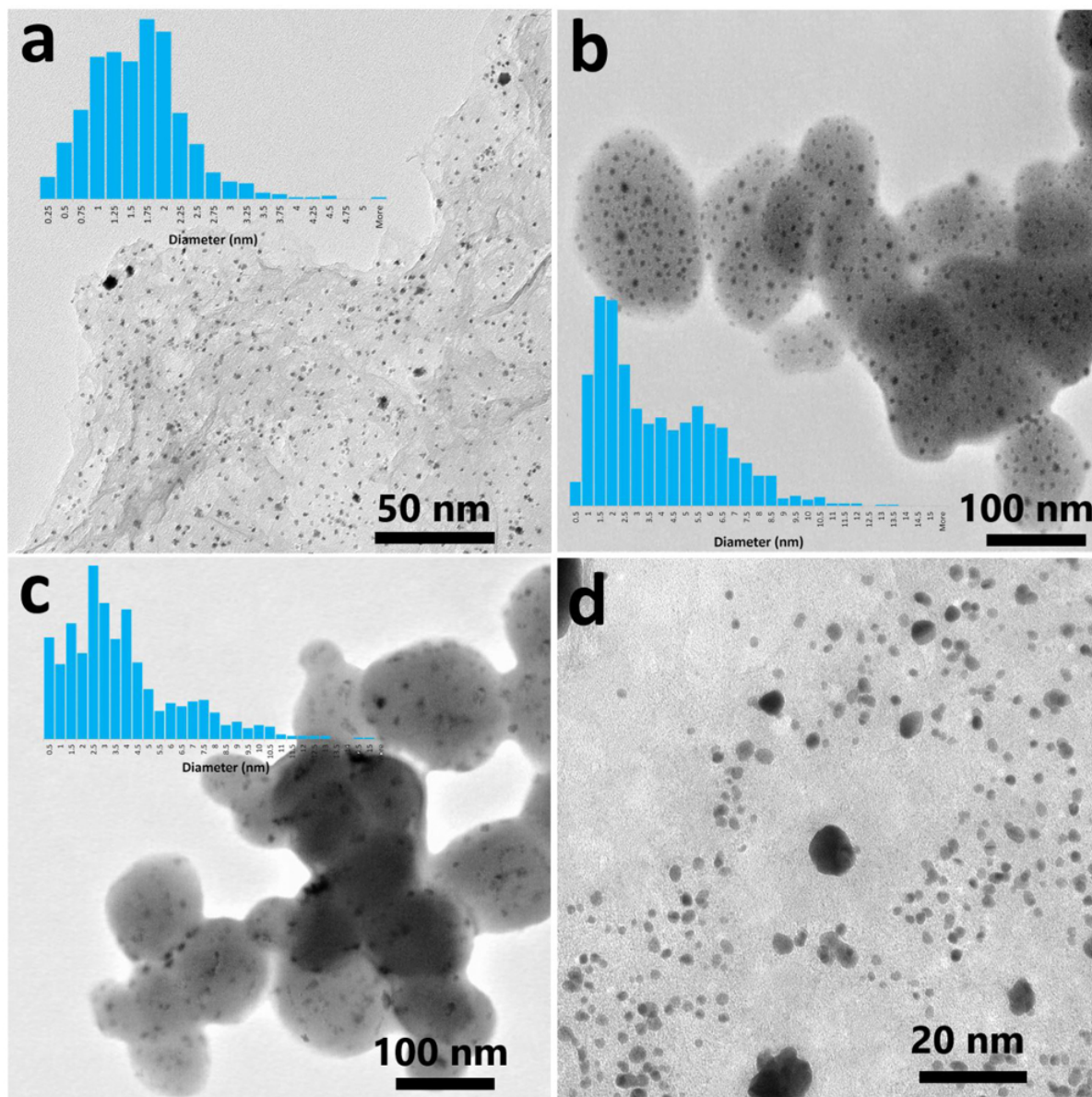


Figure 17. TEM images. (A) Pt/graphene composite produced by a 100% exposure tube (this figure has been modified from Abdolhosseinzadeh *et al.* [70]). (B) Au/TiO₂. (C) Pt/TiO₂. (D) Effect of a high IDE in the formation of large particles and the depletion of its surroundings in Pt/graphene composite.

In this work, high efficiency and accuracy of the continuous-flow photodeposition reactor for reduction of metallic cations over the surface of TiO₂ were shown by TEM images of Figure 17 (b and c). Owing to unique pulsed excitation of the substrate by limiting the exposure time (and/or UV light intensity), a very small and controlled amount of photoexcited electrons are

produced in a specific location on the substrate. Consequently, both nucleation and growth of the noble metallic nano-particles were controlled to achieve mono-dispersed and uniform distribution. These images confirm the capability of the reactor for photodeposition of different noble nano-materials over TiO₂. The mean particle sizes for panels a, b, and c in figure 17 are 1.75 nm, 3.8 nm, and 3.77nm, respectively.

Regarding to exposure time (and/or UV light intensity), it is worth to mention that photogenerated electrons have a short lifetime and, due to the poor conductivity of the photocatalyst (semiconductor), cannot move too far from the location that was generated there. Hence, in order to form a stable nucleus which should possess a minimum radius, a specific number of electrons should be generated in one excitation pulse (exposure). This implies that a minimum IDE (exposure length and/ or UV light intensity) was required to initiate the PD in the reactor. However, minimum IDE should be kept higher than the critical value needed for the formation of the nuclei. This is mainly due to the fact that the critical IDE value for the formation of stable nuclei is directly related to the quantum yield (since it is usually hard to measure the absolute quantum yield, apparent quantum yield can also be used [92]) of the photocatalyst material (0.36%-0.41% for PRGO and 0.97%-1.1% for TiO₂).

In the case of having minimum IDE, researchers can get small monodisperse particles with a uniform distribution, but the production time will also increase significantly. On the other hand, by increasing the IDE (either the exposure length or the UV light intensity), growth will dominate the nucleation (similar to the conventional photodeposition methods) and large particles will form. In very high IDEs, a formed particle may suck the electrons from its vicinity (since it has a better conductivity) and disfavor the formation of other nuclei around it. In Figure 17D, it is shown that the particle was grown enormously, and the particle size distribution of the final product are very wide.

4.5 X-ray Photoelectron Spectroscopy for the Reduction Confirmation

XPS is one of the most powerful techniques for confirming the formation of metallic nano-particles and study their chemical states. For this purpose, both survey spectra and high-resolution spectra (of Pt_{4f} and Au_{4f}) were recorded. In figure 18, complete reduction of the metallic cations and successful deposition of the noble metallic nano-particles were confirmed. For the deconvolution of both Pt_{4f} and Au_{4f}, initially, a Shirley background subtraction was

performed. Afterward, the core-level spectra were decomposed into their components with mixed Gaussian/Lorentzian (70% Gaussian and 30% Lorentzian) lines by a nonlinear least-squares curve-fitting procedure, using the XPSPEAK 4.1 software. The reduced chi-square value for all the fittings was kept below 0.01. The binding energy separation of the Pt_{4f7/2} and Pt_{4f5/2} peaks was set to 3.33 eV and the intensity ratio between the Pt_{4f7/2} and Pt_{4f5/2} peaks was set to 0.75. Those values for Au_{4f7/2} and Au_{4f5/2} were 3.71 eV and 0.78 eV, respectively.

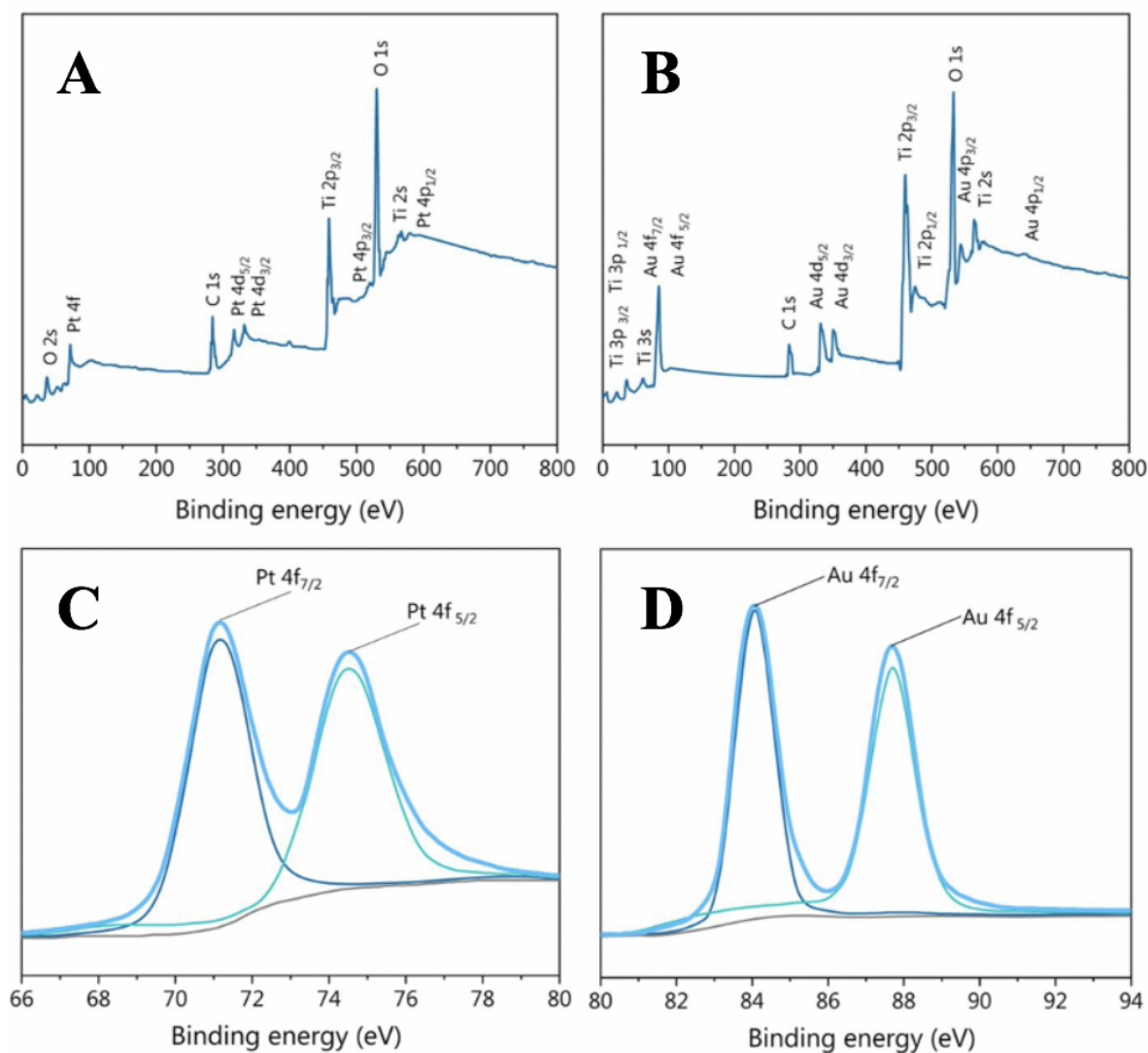


Figure 18. XPS survey spectra. Spectra for the (A) Pt/TiO₂ composite, and (B) Au/TiO₂ composite. Deconvoluted spectra for (C) Pt4f in the Pt/TiO₂ composite, and (D) Au4f in the Au/TiO₂ composite.

Deconvolution of the high-resolution Pt_{4f} and Au_{4f} peaks revealed no nonmetallic components, which verifies that the photocatalytic reduction method with TiO₂ can completely reduce the Pt⁴⁺ and Au³⁺ to Pt⁰ and Au⁰, respectively.

4.6 Inductively Coupled Plasma-Optical Emission Spectrometry (ICP-OES) for Monitoring Photodeposition Rate

In the photocatalytic deposition of noble nano-particles, since photoexcited electrons are responsible for the reduction of metallic cations, the reaction progress (NNP loading) can be studied by monitoring the concentration changes of the metallic cations. Inductively coupled plasma-optical emission spectrometry (ICP-OES) is one of the most accurate techniques for determining the cations concentration. The direct relation of the photodeposition with IDE is clearly shown in these experiments, which provide significant insights and information for understanding the working mechanism of the developed reactor (Figure 19).

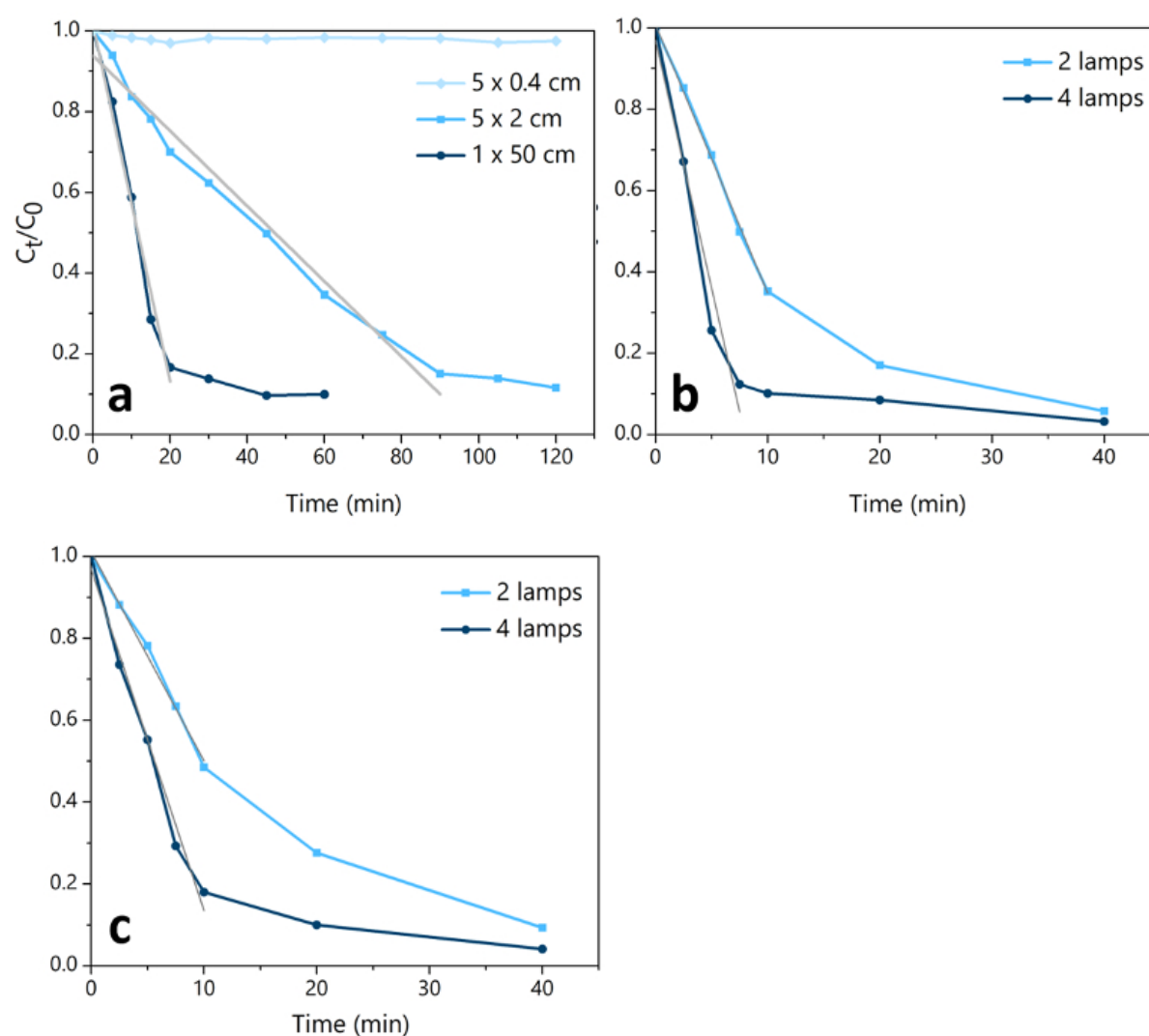


Figure 19. Concentration changes of the metallic cations during the PD in the developed reactor with various IDEs. Changes in (A) Pt/graphene, (B) Au/TiO₂, and (C) Pt/TiO₂.

Interestingly, by comparing the photodeposition rate (obtained from the ICP-OES results) for different synthesis conditions (Table 1), a direct relation between the number of photoexcited electrons and the amount of the deposited noble nano-particles can be demonstrated. The working mechanism for photodeposition of the developed reactor is also explained based on this data set.

Table 1. Effect of UV exposure length on photodeposition rate of Pt on graphene and effect of UV illumination power on photodeposition rate of Au/Pt on TiO₂.

System	Pt/graphene			Au/ TiO ₂	Au/ TiO ₂	Pt/ TiO ₂	Pt/ TiO ₂
	5 x 0.4 cm	5 x 2 cm	1 x 50 cm	2 lamps	4 lamps	2 lamps	4 lamps
Slope in the linear region	~ 0	-0.00932	-0.04412	-0.066	-0.12170	-0.05112	-0.08332

When the number of photoexcited electrons (per exposure) are larger than the value needed for a stable nucleus formation, as shown in Figure 19 and Table 1, the photodeposition rate (monitored by ICP-OES) has a linear relation with the exposure time and UV light intensity. Even when comparing the Au/TiO₂ and Pt/TiO₂ systems, since Pt⁴⁺ needs one more electron than Au³⁺, the photodeposition rate is higher (1.46) for Au/TiO₂ (the expected ratio is 4/3 = 1.33). It should be mentioned here that in some cases, the obtained PD rate ratios have slight differences with the expected values (especially for Pt), which is probably due to the fact that the proposed simple model for the nucleation and growth in the PD systems presented here is not completely valid in multi electron reductions, and other parameters should also be taken into account. At the final stages of the PD in all the systems (Figure 19), an abrupt change in the deposition rate has happened, which implies that a significant change in the deposition process has occurred. This is due to the fact that in the proposed model, it was assumed (but not specifically stated) that for each photogenerated electron, a metallic cation will be available immediately to consume it, which is apparently not the case when concentrations of the metal cations fall below a specific value (the diffusion of the cations should also be taken into account).

Since this deviation from the linear behavior occurs in low concentrations, where the major part of the cations is deposited, and the deposition of the remaining cations will require much more time, it is reasonable to conduct the PD in the linear region and recover the remaining cations from the solution by the well-developed hydrometallurgical extraction methods [93].

Conclusions

5 Conclusions

In this thesis, by considering the aforementioned discussions, it is clear that by minimizing the IDE (but keeping it higher than the critical value needed for the formation of the nuclei), researchers can get small monodisperse particles with a uniform distribution, but the production time will also increase significantly. For instance, as also shown in Figure 17, the time required for obtaining the same amount of Pt loading in the Pt/graphene system when using the 5 cm x 2 cm and 1 cm x 50 cm tubes is approximately five times longer (in the linear region). On the other hand, by increasing the IDE (either the exposure length or the UV light intensity), growth will dominate the nucleation (similar to the conventional PD methods) and large particles will form.

In very high IDEs, a formed particle may suck the electrons from its vicinity (since it has a better conductivity) and disfavor the formation of other nuclei around it. In this case, the particle grows enormously, and the particle size distribution of the final product will be very wide. This phenomenon is more problematic in high quantum-yield photocatalysts (comparing TiO₂ with PRGO), and proper IDE adjustment is more challenging.

As a result, shorter exposure lengths and a lower illumination dose (number of the UV lamps) are used for TiO₂-based composites and still, as can be seen in TEM images, the graphene-based composite has a better monodispersity than the two other TiO₂-based composites. Hence, the IDE should be carefully optimized to get the highest quality product with the highest yield. The results and discussions presented in this project clearly demonstrate the potential and abilities of the developed reactor for a precisely controlled synthesis of noble nano-particles catalysts (on both types of substrates) on a large scale with low cost and in a continuous manner.

References

6 References

1. Clark, W. C.; Vondjidis, A. G. *An infrared study of the photocatalytic reaction between titanium dioxide and silver nitrate*. *J. Catal.* 1965, **4** (6), 691–696..
2. Kraeutler, B. and A.J. Bard, *Heterogeneous photocatalytic preparation of supported catalysts. Photodeposition of platinum on titanium dioxide powder and other substrates*. *Journal of the American Chemical Society*, 1978. **100**(13): p. 4317-4318.
3. Kudo, A. and Y. Miseki, *Heterogeneous photocatalyst materials for water splitting*. *Chem Soc Rev*, 2009. **38**(1): p. 253-78.
4. Maeda, K., *Photocatalytic water splitting using semiconductor particles: History and recent developments*. *Journal of Photochemistry and Photobiology C: Photochemistry Reviews*, 2011. **12**(4): p. 237-268.
5. Roy, S.C., et al., *Toward solar fuels: photocatalytic conversion of carbon dioxide to hydrocarbons*. *ACS Nano*, 2010. **4**(3): p. 1259-78.
6. Chong, M.N., et al., *Recent developments in photocatalytic water treatment technology: a review*. *Water Res*, 2010. **44**(10): p. 2997-3027.
7. Ahmed, S., et al., *Heterogeneous photocatalytic degradation of phenols in wastewater: A review on current status and developments*. *Desalination*, 2010. **261**(1-2): p. 3-18.
8. Bamwenda, G. R.; Tsubota, S.; Nakamura, T.; Haruta, M. Photoassisted hydrogen production from a water-ethanol solution: a comparison of activities of Au-TiO₂ and Pt-TiO₂. *J. Photochem. Photobiol., A* 1995, **89** (2), 177–189.
9. Kang, J.-G. and Y. Sohn, *Interfacial nature of Ag nanoparticles supported on TiO₂ photocatalysts*. *Journal of Materials Science*, 2011. **47**(2): p. 824-832.
10. Ma, L.L., et al., *The fabrication of SnSe/Ag nanoparticles on TiO₂ nanotubes*. *Materials Science and Engineering: B*, 2013. **178**(1): p. 77-82.
11. Maeda, K., R. Abe, and K. Domen, *Role and Function of Ruthenium Species as Promoters with TaON-Based Photocatalysts for Oxygen Evolution in Two-Step Water Splitting under Visible Light*. *The Journal of Physical Chemistry C*, 2011. **115**(7): p. 3057-3064.
12. Murata, A., et al., *Visible-Light Active Photocatalytic WO₃ Films Loaded with Pt Nanoparticles Deposited by Sputtering*. *Journal of Nanoscience and Nanotechnology*, 2012. **12**(6): p. 5082-5086.
13. Dasgupta, N.P., et al., *Atomic layer deposition of platinum catalysts on nanowire surfaces for photoelectrochemical water reduction*. *J Am Chem Soc*, 2013. **135**(35): p. 12932-5.
14. Busser, G.W., B. Mei, and M. Muhler, *Optimizing the deposition of hydrogen evolution sites on suspended semiconductor particles using on-line photocatalytic reforming of aqueous methanol solutions*. *ChemSusChem*, 2012. **5**(11): p. 2200-6.
15. Rufus, I. B.; Viswanathan, B.; Ramakrishnan, V.; Kuriacose, J. C. Cadmium sulfide with iridium sulfide and platinum sulfide deposits as a photocatalyst for the decomposition of aqueous sulfide. *J. Photochem. Photobiol., A* 1995, **91** (1), 63–66..
16. Chen, X., et al., *In situ photodeposition of NiOX on CdS for hydrogen production under visible light: Enhanced activity by controlling solution environment*. *Applied Catalysis B: Environmental*, 2014. **152-153**: p. 68-72.
17. Jiang, X., et al., *Photocatalytic reforming of glycerol for H₂ evolution on Pt/TiO₂: fundamental understanding the effect of co-catalyst Pt and the Pt deposition route*. *Journal of Materials Chemistry A*, 2015. **3**(5): p. 2271-2282.

18. Wenderich, K. and G. Mul, *Methods, Mechanism, and Applications of Photodeposition in Photocatalysis: A Review*. Chem Rev, 2016. **116**(23): p. 14587-14619.
19. Nakamatsu, H.; Kawai, T.; Koreeda, A.; Kawai, S. Electronmicroscopic observation of photodeposited Pt on TiO₂ particles in relation to photocatalytic activity. J. Chem. Soc., Faraday Trans. 1 1986, **82** (2), 527–531.
20. Kraeutler, B.; Bard, A. J. Heterogeneous photocatalytic preparation of supported catalysts. Photodeposition of platinum on titanium dioxide powder and other substrates. J. Am. Chem. Soc. 1978, **100** (13), 4317– 4318.
21. Qamar, M.; Ganguli, A. K. Self-assembling behaviour of Pt nanoparticles onto surface of TiO₂ and their resulting photocatalytic activity. Bull. Mater. Sci. 2013, **36** (6), 945–951.
22. Murcia, J.J., J.A. Navío, and M.C. Hidalgo, *Insights towards the influence of Pt features on the photocatalytic activity improvement of TiO₂ by platinisation*. Applied Catalysis B: Environmental, 2012. **126**: p. 76-85.
23. Chowdhury, P., et al., *Sacrificial Hydrogen Generation from Formaldehyde with Pt/TiO₂ Photocatalyst in Solar Radiation*. Industrial & Engineering Chemistry Research, 2013. **52**(14): p. 5023-5029.
24. Li, Y.; Lu, G.; Li, S. Photocatalytic hydrogen generation and decomposition of oxalic acid over platinized TiO₂. Appl. Catal., A 2001, **214** (2), 179–185..
25. Piwoński, I., et al., *The effect of the deposition parameters on size, distribution and antimicrobial properties of photoinduced silver nanoparticles on titania coatings*. Applied Surface Science, 2011. **257**(16): p. 7076-7082.
26. Iliev, V., et al., *Influence of the size of gold nanoparticles deposited on TiO₂ upon the photocatalytic destruction of oxalic acid*. Journal of Molecular Catalysis A: Chemical, 2007. **263**(1-2): p. 32-38.
27. Oros-Ruiz, S., et al., *Effect of Gold Particle Size and Deposition Method on the Photodegradation of 4-Chlorophenol by Au/TiO₂*. Topics in Catalysis, 2011. **54**(8-9): p. 519-526.
28. Kriek, R.J. and F. Mahlamvana, *Dependency on chloride concentration and ‘in-sphere’ oxidation of H₂O for the effective TiO₂-photocatalysed electron transfer from H₂O to [PdCl_n(H₂O)_{4-n}]²⁻ⁿ (n=0–4) in the absence of an added sacrificial reducing agent*. Applied Catalysis A: General, 2012. **423-424**: p. 28-33.
29. Borgarello, E., et al., *Light-induced reduction of rhodium(III) and palladium(II) on titanium dioxide dispersions and the selective photochemical separation and recovery of gold(III), platinum(IV), and rhodium(III) in chloride media*. Inorganic Chemistry, 1986. **25**(25): p. 4499-4503.
30. Ohno, T., K. Sarukawa, and M. Matsumura, *Crystal faces of rutile and anatase TiO₂ particles and their roles in photocatalytic reactions*. New Journal of Chemistry, 2002. **26**(9): p. 1167-1170.
31. Li, C., et al., *Photohole-oxidation-assisted anchoring of ultra-small Ru clusters onto TiO₂ with excellent catalytic activity and stability*. Journal of Materials Chemistry A, 2013. **1**(7).
32. Khnayzer, R.S., et al., *Structure and Activity of Photochemically Deposited “CoPi” Oxygen Evolving Catalyst on Titania*. ACS Catalysis, 2012. **2**(10): p. 2150-2160.
33. Zhu, H., et al., *Construction of Z-scheme type CdS–Au–TiO₂ hollow nanorod arrays with enhanced photocatalytic activity*. Applied Catalysis B: Environmental, 2009. **90**(3-4): p. 463-469.

34. Kim, M., et al., *Efficient visible light-induced H₂ production by Au@CdS/TiO₂ nanofibers: Synergistic effect of core-shell structured Au@CdS and densely packed TiO₂ nanoparticles*. Applied Catalysis B: Environmental, 2015. **166-167**: p. 423-431.
35. Zhou, H., et al., *Biomass-derived hierarchical porous CdS/M/TiO₂ (M = Au, Ag, Pt, Pd) ternary heterojunctions for photocatalytic hydrogen evolution*. International Journal of Hydrogen Energy, 2014. **39**(29): p. 16293-16301.
36. Tanaka, A., et al., *Functionalization of Au/TiO₂ Plasmonic Photocatalysts with Pd by Formation of a Core-Shell Structure for Effective Dechlorination of Chlorobenzene under Irradiation of Visible Light*. The Journal of Physical Chemistry C, 2013. **117**(33): p. 16983-16989.
37. Herrmann, J. M.; Disdier, J.; Pichat, P.; Fernández, A.; González-Eliphe, A.; Munuera, G.; Leclercq, C. Titania-supported bimetallic catalyst synthesis by photocatalytic codeposition at ambient temperature: preparation and characterization of Pt-Rh, Ag-Rh, and Pt-Pd couples. J. Catal. 1991, **132** (2), 490–497.
38. Qiao, P., et al., *A general synthesis strategy of multi-metallic nanoparticles within mesoporous titania via in situ photo-deposition*. J. Mater. Chem. A, 2014. **2**(41): p. 17321-17328.
39. Fujii, M., et al., *Photodeposition of CdS Quantum Dots on TiO₂: Preparation, Characterization, and Reaction Mechanism*. The Journal of Physical Chemistry C, 2009. **113**(38): p. 16711-16716.
40. Zhao, W.; Chen, C.; Li, X.; Zhao, J.; Hidaka, H.; Serpone, N. Photodegradation of sulforhodamine-B dye in platinized titania dispersions under visible light irradiation: influence of platinum as a functional co-catalyst. J. Phys. Chem. B 2002, **106** (19), 5022–5028.
41. Sclafani, A.; Mozzanega, M. N.; Pichat, P. Effect of silver deposits on the photocatalytic activity of titanium dioxide samples for the dehydrogenation or oxidation of 2-propanol. J. Photochem. Photobiol., A 1991, **59** (2), 181–189.
42. Xi, C.; Chen, Z.; Li, Q.; Jin, Z. Effects of H⁺, Cl⁻ and CH₃COOH on the photocatalytic conversion of PtCl₆²⁻ in aqueous TiO₂ dispersion. J. Photochem. Photobiol., A 1995, **87** (3), 249–255.
43. Mahlamvana, F. and R.J. Kriek, *Photocatalytic reduction of platinum(II and IV) from their chloro complexes in a titanium dioxide suspension in the absence of an organic sacrificial reducing agent*. Applied Catalysis B: Environmental, 2014. **148-149**: p. 387-393.
44. Zhang, F., et al., *Synthesis of titania-supported platinum catalyst: the effect of pH on morphology control and valence state during photodeposition*. Langmuir, 2004. **20**(21): p. 9329-34.
45. Herrmann, J. M.; Disdier, J.; Pichat, P. Photoassisted platinum deposition on TiO₂ powder using various platinum complexes. J. Phys. Chem. 1986, **90** (22), 6028–6034.
46. Teramura, K., et al., *In Situ Time-Resolved Energy-Dispersive XAFS Study on Photodeposition of Rh Particles on a TiO₂ Photocatalyst*. The Journal of Physical Chemistry C, 2008. **112**(23): p. 8495-8498.
47. Liu, Y., S. Wei, and W. Gao, *Ag/ZnO heterostructures and their photocatalytic activity under visible light: effect of reducing medium*. J Hazard Mater, 2015. **287**: p. 59-68.
48. Huang, Q., et al., *Selective synthesis of different ZnO/Ag nanocomposites as surface enhanced Raman scattering substrates and highly efficient photocatalytic catalysts*. RSC Advances, 2015. **5**(34): p. 27075-27081.

49. Wang, J., et al., *Largely improved photocatalytic properties of Ag/tetrapod-like ZnO nanocompounds prepared with different PEG contents*. Applied Surface Science, 2011. **257**(17): p. 7763-7770.
50. Lin, C.Y., et al., *Electrode modified with a composite film of ZnO nanorods and Ag nanoparticles as a sensor for hydrogen peroxide*. Talanta, 2010. **82**(1): p. 340-7.
51. Park, S., et al., *Photoreaction of gold ions from potassium gold cyanide wastewater using solution-combusted ZnO nanopowders*. Journal of the European Ceramic Society, 2010. **30**(2): p. 177-180.
52. Carabineiro, S.A.C., et al., *Catalytic performance of Au/ZnO nanocatalysts for CO oxidation*. Journal of Catalysis, 2010. **273**(2): p. 191-198.
53. Lu, L., et al., *Photoinduced growth of Cu nanoparticles on ZnO from CuCl₂ in methanol*. Journal of Nanoparticle Research, 2006. **9**(3): p. 491-496.
54. Naknam, P., A. Luengnaruemitchai, and S. Wongkasemjit, *Preferential CO oxidation over Au/ZnO and Au/ZnO-Fe₂O₃ catalysts prepared by photodeposition*. International Journal of Hydrogen Energy, 2009. **34**(24): p. 9838-9846.
55. Wu, M., et al., *In situ growth of matchlike ZnO/Au plasmonic heterostructure for enhanced photoelectrochemical water splitting*. ACS Appl Mater Interfaces, 2014. **6**(17): p. 15052-60.
56. He, W., et al., *Photogenerated charge carriers and reactive oxygen species in ZnO/Au hybrid nanostructures with enhanced photocatalytic and antibacterial activity*. J Am Chem Soc, 2014. **136**(2): p. 750-7.
57. Su, L. and N. Qin, *A facile method for fabricating Au-nanoparticles-decorated ZnO nanorods with greatly enhanced near-band-edge emission*. Ceramics International, 2015. **41**(2): p. 2673-2679.
58. Chang, C.M., M.H. Hon, and I.C. Leu, *Outstanding H₂ sensing performance of Pd nanoparticle-decorated ZnO nanorod arrays and the temperature-dependent sensing mechanisms*. ACS Appl Mater Interfaces, 2013. **5**(1): p. 135-43.
59. Chang, C.-M., M.-H. Hon, and I.-C. Leu, *Improvement in CO sensing characteristics by decorating ZnO nanorod arrays with Pd nanoparticles and the related mechanisms*. RSC Advances, 2012. **2**(6).
60. Liqiang, J., et al., *Investigations on the surface modification of ZnO nanoparticle photocatalyst by depositing Pd*. Journal of Solid State Chemistry, 2004. **177**(11): p. 4221-4227.
61. Jin, Y., et al., *An ultra-low Pd loading nanocatalyst with efficient catalytic activity*. Nanoscale, 2015. **7**(12): p. 5510-5.
62. Gomathisankar, P., et al., *Enhanced photocatalytic hydrogen production from aqueous methanol solution using ZnO with simultaneous photodeposition of Cu*. International Journal of Hydrogen Energy, 2013. **38**(27): p. 11840-11846.
63. Tan, C., X. Huang, and H. Zhang, *Synthesis and applications of graphene-based noble metal nanostructures*. Materials Today, 2013. **16**(1-2): p. 29-36.
64. Chang, G., et al., *Synthesis of highly dispersed Pt nanoclusters anchored graphene composites and their application for non-enzymatic glucose sensing*. Electrochimica Acta, 2015. **157**: p. 149-157.
65. Yoo, E., et al., *Enhanced electrocatalytic activity of Pt subnanoclusters on graphene nanosheet surface*. Nano Lett, 2009. **9**(6): p. 2255-9.
66. Shang, N., et al., *Platinum Integrated Graphene for Methanol Fuel Cells*. The Journal of Physical Chemistry C, 2010. **114**(37): p. 15837-15841.

67. Maiyalagan, T., et al., *Electrodeposited Pt on three-dimensional interconnected graphene as a free-standing electrode for fuel cell application*. Journal of Materials Chemistry, 2012. **22**(12).
68. Rao, C. and D. Trivedi, *Chemical and electrochemical depositions of platinum group metals and their applications*. Coordination Chemistry Reviews, 2005. **249**(5-6): p. 613-631.
69. Kondratiev, V.V., V.V. Malev, and S.N. Eliseeva, *Composite electrode materials based on conducting polymers loaded with metal nanostructures*. Russian Chemical Reviews, 2016. **85**(1): p. 14-37.
70. Abdolhosseinzadeh, S., S. Sadighikia, and S. Alkan Gürsel, *Scalable Synthesis of Sub-Nanosized Platinum-Reduced Graphene Oxide Composite by an Ultraprecise Photocatalytic Method*. ACS Sustainable Chemistry & Engineering, 2018. **6**(3): p. 3773-3782.
71. Maeda, K.; Lu, D.; Teramura, K.; Domen, K. Direct deposition of nanoparticulate rhodium-chromium mixed-oxides on a semiconductor powder by band-gap irradiation. J. Mater. Chem. 2008, **18** (30), 3539– 3542.
72. Busser, G.W., et al., *Photodeposition of copper and chromia on gallium oxide: the role of co-catalysts in photocatalytic water splitting*. ChemSusChem, 2014. **7**(4): p. 1030-4.
73. Kudo, A.; Omori, K.; Kato, H. A novel aqueous process for preparation of crystal form-controlled and highly crystalline BiVO₄ powder from layered vanadates at room temperature and its photocatalytic and photophysical properties. J. Am. Chem. Soc. 1999, **121** (49), 11459–11467.
74. Kudo, A.; Ueda, K.; Kato, H.; Mikami, I. Photocatalytic O₂ evolution under visible light irradiation on BiVO₄ in aqueous AgNO₃ solution. Catal. Lett. 1998, **53** (3–4), 229–230.
75. Tokunaga, S.; Kato, H.; Kudo, A. Selective preparation of monoclinic and tetragonal BiVO₄ with scheelite structure and their photocatalytic properties. Chem. Mater. 2001, **13** (12), 4624–4628.
76. Yu, S.-C., et al., *A novel membrane reactor for separating hydrogen and oxygen in photocatalytic water splitting*. Journal of Membrane Science, 2011. **382**(1-2): p. 291-299.
77. Zhang, X., et al., *Preparation of Ag doped BiVO₄ film and its enhanced photoelectrocatalytic (PEC) ability of phenol degradation under visible light*. J Hazard Mater, 2009. **167**(1-3): p. 911-4.
78. Kohtani, S., et al., *Adsorptive and photocatalytic properties of Ag-loaded BiVO₄ on the degradation of 4-n-alkylphenols under visible light irradiation*. Catalysis Communications, 2005. **6**(3): p. 185-189.
79. Zhou, C., et al., *Mesoporous plasmonic Au-loaded Ta₂O₅ nanocomposites for efficient visible light photocatalysis*. Catalysis Today, 2014. **225**: p. 158-163.
80. Takahara, Y.; Kondo, J. N.; Takata, T.; Lu, D.; Domen, K. Mesoporous tantalum oxide. 1. Characterization and photocatalytic activity for the overall water decomposition. Chem. Mater. 2001, **13** (4), 1194–1199.
81. Sayama, K.; Arakawa, H. Effect of Na₂CO₃ addition on photocatalytic decomposition of liquid water over various semiconductor catalysis. J. Photochem. Photobiol., A 1994, **77** (2–3), 243–247.
82. Ishii, T., H. Kato, and A. Kudo, *H₂ evolution from an aqueous methanol solution on SrTiO₃ photocatalysts codoped with chromium and tantalum ions under visible light*

- irradiation*. Journal of Photochemistry and Photobiology A: Chemistry, 2004. **163**(1-2): p. 181-186.
83. Sulaeman, U., S. Yin, and T. Sato, *Solvothermal synthesis and photocatalytic properties of chromium-doped SrTiO₃ nanoparticles*. Applied Catalysis B: Environmental, 2011. **105**(1-2): p. 206-210.
 84. Kang, H.W., et al., *Organic-inorganic composite of g-C₃N₄-SrTiO₃:Rh photocatalyst for improved H₂ evolution under visible light irradiation*. International Journal of Hydrogen Energy, 2012. **37**(16): p. 11602-11610.
 85. Yoshida, M., et al., *In situ observation of carrier transfer in the Mn-oxide/Nb:SrTiO₃ photoelectrode by X-ray absorption spectroscopy*. Chem Commun (Camb), 2013. **49**(71): p. 7848-50.
 86. Tanaka, R., et al., *Photo-Electrochemical Synthesis of Silver-Oxide Clathrate Ag₇O₈NO₃ on SrTiO₃*. Electrochemical and Solid-State Letters, 2012. **15**(4).
 87. Sasaki, Y., et al., *The effect of co-catalyst for Z-scheme photocatalysis systems with an Fe³⁺/Fe²⁺ electron mediator on overall water splitting under visible light irradiation*. Journal of Catalysis, 2008. **259**(1): p. 133-137.
 88. Lee, W.-H., et al., *A novel twin reactor for CO₂ photoreduction to mimic artificial photosynthesis*. Applied Catalysis B: Environmental, 2013. **132-133**: p. 445-451.
 89. Liu, J., et al., *Photocatalytic hydrogen production from water/methanol solutions over highly ordered Ag-SrTiO₃ nanotube arrays*. International Journal of Hydrogen Energy, 2011. **36**(10): p. 5811-5816.
 90. Sun, Y., J. Liu, and Z. Li, *Design of highly ordered Ag-SrTiO₃ nanotube arrays for photocatalytic degradation of methyl orange*. Journal of Solid State Chemistry, 2011. **184**(8): p. 1924-1930.
 91. Abdolhosseinzadeh, S., et al., *A Continuous-flow Photocatalytic Reactor for the Precisely Controlled Deposition of Metallic Nanoparticles*. J Vis Exp, 2019(146).
 92. de Sá, D.S., et al., *Intensification of photocatalytic degradation of organic dyes and phenol by scale-up and numbering-up of meso- and microfluidic TiO₂ reactors for wastewater treatment*. Journal of Photochemistry and Photobiology A: Chemistry, 2018. **364**: p. 59-75.
 93. Kononova, O.N., et al., *Ion exchange recovery of platinum from chloride solutions*. Hydrometallurgy, 2010. **100**(3-4): p. 161-167.